Cell Reports

Article

A naturally occurring mutation in ATP synthase subunit c is associated with increased damage following hypoxia/reoxygenation in STEMI patients

Graphical abstract

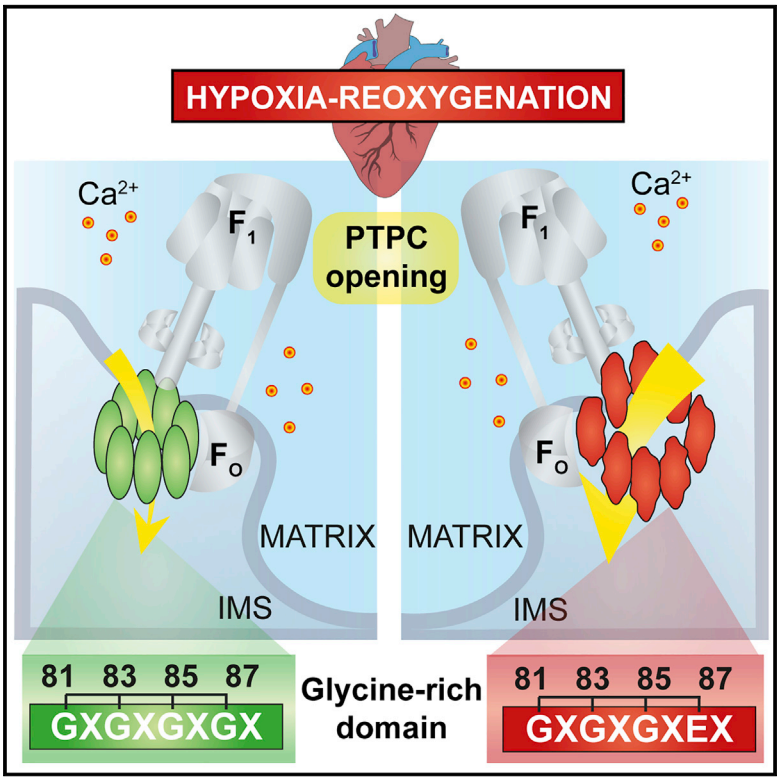

Authors

Giampaolo Morciano, Gaia Pedriali, Massimo Bonora, ..., Lorenzo Galluzzi, Gianluca Campo, Paolo Pinton

Correspondence

paolo.pinton@unife.it

In brief

Studies in humans about the deleterious effects of PTPC opening in ischemia/reperfusion should be improved. Here, Morciano et al. identify a naturally occurring mutation in the subunit c that exacerbates the hypoxia/reoxygenation damage in human cardiomyocytes. Moreover, they report the correlation between PTPC opening and reperfusion injury in STEMI patients.

Highlights

- G87E of ATP synthase subunit c is harmful under stressful conditions in humans
- G87E increases PTPC opening
- G87E worsens hypoxia/reoxygenation damage in STEMI patients
- PTPC opening is positively related to reperfusion injury in STEMI patients

Morciano et al., 2021, Cell Reports *35*, 108983
April 13, 2021
https://doi.org/10.1016/j.celrep.2021.108983

CellPress

Cell Reports

CellPress
OPEN ACCESS

Article

A naturally occurring mutation in ATP synthase subunit c is associated with increased damage following hypoxia/reoxygenation in STEMI patients

Giampaolo Morciano,[1,2] Gaia Pedriali,[1] Massimo Bonora,[2] Rita Pavasini,[3] Elisa Mikus,[4] Simone Calvi,[4] Matteo Bovolenta,[5] Magdalena Lebiedzinska-Arciszewska,[7] Mirko Pinotti,[6] Alberto Albertini,[4] Mariusz R. Wieckowski,[7] Carlotta Giorgi,[2] Roberto Ferrari,[1,3] Lorenzo Galluzzi,[8,9,10,11,12] Gianluca Campo,[1,3] and Paolo Pinton[1,2,13,*]

[1]Maria Cecilia Hospital, GVM Care & Research, 48033 Cotignola, Ravenna, Italy
[2]Department of Medical Sciences, Section of Experimental Medicine, Laboratory for Technologies of Advanced Therapies (LTTA), University of Ferrara, 44121 Ferrara, Italy
[3]Cardiovascular Institute, Azienda Ospedaliero-Universitaria di Ferrara, Cona, 44121 Ferrara, Italy
[4]Cardiothoracic and Vascular Department, Maria Cecilia Hospital, GVM Care & Research, 48033 Cotignola, Ravenna, Italy
[5]Genethon, INSERM UMR951, 1 bis, rue de l'Internationale BP60, 91002 Evry Cedex, France
[6]Department of Life Sciences and Biotechnology, University of Ferrara, 44121 Ferrara, Italy
[7]Laboratory of Mitochondrial Biology and Metabolism, Nencki Institute of Experimental Biology, Polish Academy of Sciences, Warsaw, Poland
[8]Department of Radiation Oncology, Weill Cornell Medical College, New York, NY, USA
[9]Sandra and Edward Meyer Cancer Center, New York, NY, USA
[10]Caryl and Israel Englander Institute for Precision Medicine, New York, NY, USA
[11]Department of Dermatology, Yale School of Medicine, New Haven, CT, USA
[12]Université de Paris, Paris, France
[13]Lead contact
*Correspondence: paolo.pinton@unife.it
https://doi.org/10.1016/j.celrep.2021.108983

SUMMARY

Preclinical models of ischemia/reperfusion injury (RI) demonstrate the deleterious effects of permeability transition pore complex (PTPC) opening in the first minutes upon revascularization of the occluded vessel. The ATP synthase c subunit (Csub) influences PTPC activity in cells, thus impacting tissue injury. A conserved glycine-rich domain in Csub is classified as critical because, when mutated, it modifies ATP synthase properties, protein interaction with the mitochondrial calcium (Ca^{2+}) uniporter complex, and the conductance of the PTPC. Here, we document the role of a naturally occurring mutation in the Csub-encoding *ATP5G1* gene at the G87 position found in two ST-segment elevation myocardial infarction (STEMI) patients and how PTPC opening is related to RI in patients affected by the same disease. We report a link between the expression of ATP5G1^{G87E} and the response to hypoxia/reoxygenation of human cardiomyocytes, which worsen when compared to those expressing the wild-type protein, and a positive correlation between PTPC and RI.

INTRODUCTION

Although timely reperfusion is essential for the functional recovery of ischemic myocardium, it has been suggested that, especially when it occurs late, reperfusion can contribute to further myocyte death and damage (Ferrari et al., 2017).

The existence of reperfusion damage has been the subject of several controversies. It was argued that, at best, the damage detected immediately after reperfusion represents just an acceleration of the injury that would have occurred if the myocardium had never been reperfused. However, experimental data show that it is possible to reduce the damage induced by reperfusion with interventions applied just at the time of revascularization. These interventions (i.e., calcium [Ca^{2+}] antagonists, antioxidants, and sodium-hydrogen exchange inhibitors) are aimed at reducing the possible cause of reperfusion damage, mainly readmission of Ca^{2+}, oxygen, pH (Giorgi et al., 2018; Morciano et al., 2015; Santulli et al., 2015), and other targets (Paradies et al., 2018). All the abovementioned mechanisms and interventions, when explored alone, failed to play a clinical role, as they are most likely not mutually exclusive but instead play a synergic role.

A possible common pathway has been identified in the opening of the mitochondrial permeability transition pore complex (PTPC) (Chinopoulos, 2017). This is a nonselective channel where a still undefined number of mitochondrial proteins interact to form a structural and functional network across mitochondrial inner and outer membranes, which, under physiological conditions, quickly flickers between the open and closed conformations during ischemia and remains closed, but it opens during

reperfusion (Griffiths and Halestrap, 1995). In ischemia, cardiomyocytes are exposed to Ca^{2+} overload (Lambert et al., 2019; Luongo et al., 2017), reactive oxygen species (ROS), and inflammation, which all increase the susceptibility of the PTPC to opening, but in the presence of low pH, they do not cause its opening (Griffiths and Halestrap, 1995). Reperfusion restores a normal pH, which induces increased PTPC activity with severe mitochondrial impairment and the disruption of energy production (Bonora et al., 2019; Kwong and Molkentin, 2015), leading to massive damage.

Several attempts have been made to limit reperfusion damage in preclinical animal models and in humans by either promoting mitochondrial functions or inhibiting PTPC at the time of a primary angioplasty (Campo et al., 2017a, 2017b). The most studied therapy is cyclosporine A (CsA), as it targets the known PTPC modulator cyclophilin D (CypD) (Chinopoulos and Adam-Vizi, 2012). Unfortunately, the positive initial results (Piot et al., 2008) have not been confirmed in properly larger trials (Cung et al., 2015; Ottani et al., 2016). One criticism is that these compounds do not target the specific proteins involved in PTPC opening.

Our group and others provided evidence that the F_O-ATP synthase c subunit (Csub) is an important regulator of the PTPC (Alavian et al., 2014; Azarashvili et al., 2014; Bonora et al., 2013a, 2017; Elustondo et al., 2016; Morciano et al., 2018; Neginskaya et al., 2019); this feature is amplified when its highly conserved glycine-rich domain becomes mutated (Alavian et al., 2014; Bonora et al., 2017; Huang and Docampo, 2020). The implication of Csub in myocardial infarction (MI) is suggested by the significant correlation between the circulating protein in ST-segment elevation myocardial infarction (STEMI) patients and several surrogate markers of myocardial reperfusion (Campo et al., 2016) and that its selective targeting in the first 10 min of revascularization protects the ischemic heart from impaired cardiac performance and excessive apoptosis in animal models (Morciano et al., 2018). However, the link between reperfusion damage and the PTPC in humans remains elusive and speculative, in view of the difficulties in measuring the eventual damage following revascularization and PTPC functional activity.

To this aim, we tried to provide a useful and interesting update in this field by studying the role of a naturally occurring mutation in the glycine-rich domain of Csub (encoded by the *ATP5G1* gene) found in two patients affected by STEMI and by analyzing PTPC opening in cells from patients and the reperfusion damage caused by revascularization during primary angioplasty.

RESULTS

A naturally occurring mutation in *ATP5G1* gene

Because MI is a multifactorial disease in which both environmental factors and genetic profiles play key roles in its development, we found interesting the idea that new genetic determinants linked to PTPC may exist and could be involved in reperfusion damage following percutaneous coronary intervention (PCI).

Having interest in the study of Csub as a crucial regulator of PTPC activity in MI, we randomly selected one-third (N = 52; Table S1) of STEMI patients from those already enrolled in our previous study (Campo et al., 2016) to perform a complete genetic screening for all 3 *ATP5G1–3* genes encoding Csub of the PTPC (Table S1). The results are summarized in Table 1. We identified 23 known polymorphisms and 6 unknown variations (not reported in the gnomAD, dbSNP, and 1000 Genomes databases), of which 4 fell in noncoding genomic regions such as introns and the 5′ UTR and 2 were missense mutations. The first was a G to A nucleotide transition found in exon 3 of the *ATP5G1* gene in 2 out of 52 patients (Figure 1A); this variation led to a missense mutation (a glycine substitution with a glutamic acid, G X E) at position 87 ($ATP5G1^{G87E}$). Given that the amino acid substitution occurred in the highly conserved glycine-rich domain of the Csub coding sequence (Figure 1B), we first conducted a bioinformatics analysis to predict whether the variation, once expressed, may induce detrimental phenotypes *in vivo*. A query run in PolyPhen-2 software (Adzhubei et al., 2013) predicted $ATP5G1^{G87E}$ to be detrimental with a score of 0.993 on a scale from 0 to 1 (Figure 1C). To verify this finding, we used six other prediction software packages described in the literature, and all of them provided similar readouts, as follows: once expressed, this mutated protein would most likely be damaging, with scores ranging between 60% and 90% (Figure 1C). Additional bioinformatics studies based on the RaptorX web server (Källberg et al., 2012) also predicted that $ATP5G1^{G87E}$ would exhibit structural deformation at the level of the first helix of Csub (Figure 1D).

$ATP5G1^{G87E}$ expression aggravates PTPC-mediated H/R damage in human cardiomyocytes

We sought to confirm the putative harmful effects of $ATP5G1^{G87E}$ in human ventricular cardiomyocytes (AC16 cells) by using a combination of chemical induction of PTPC opening and a model of hypoxia/reoxygenation (H/R) to mimic reperfusion to which cells would be subjected upon PCI in STEMI patients (Bonora et al., 2016). To this end, *ATP5G1* cDNA was mutated and overexpressed in cardiomyocytes to resemble the effect of the heterozygous mutation. As shown in Figure 1E, the mutated protein was expressed and localized to the inner mitochondrial membrane compartment in AC16 cells. As expected, the expression of $ATP5G1^{G87E}$ strongly altered PTPC opening upon Ca^{2+}-dependent stimulation in three different types of cardiac myocytes, namely, AC16 cells ($p < 0.01$), neonatal rat cardiomyocytes (NRCMs; $p < 0.01$), and HL-1 cells ($p < 0.05$) (Figure 1F). In detail, $ATP5G1^{G87E}$ promoted PTPC opening at a 2-fold greater rate than that seen by overexpressing the Csub wild type (WT) ($ATP5G1^{WT}$) (Bonora et al., 2013a). These data were confirmed in Figure 1G, in which a drop in mitochondrial membrane potential was recorded following oxidative-stress-dependent PTPC opening. AC16 was used in the experiments reported below because this cell line has a human origin, is derived from the ventricle, and is easy to handle.

To validate the hypothesis that genetic determinants of myocardial Csub are critical factors at the time of reperfusion, we took advantage of a hypoxic chamber, by which we evaluated the kinetics of the PTPC during H/R. Even in this case, cells expressing $ATP5G1^{G87E}$ exhibited hyperresponsive PTPC opening ($p < 0.01$; Figure 2A) compared with those

Table 1. Results from next-generation sequencing applied to all ATP5G1–3 genes in study population C

ATPG1	Variation	Coordinates	Functional position	dbSNP
Exon 1	G > T	chr17:46970684	intronic	rs573172017
Exon 3	ΔCTCT	chr17:46972481-46972484	intronic	rs3080082
	G > A	chr17:46972660	exonic (missense)	–
Exon 4	C > T	chr17:46972865	intronic	rs832410
	T > C	chr17:46973103	exonic (missense)	–
ATPG2				
Exon 1	ins.CA	chr12:54070063	5′ UTR	rs4020138
	C > T	chr12:54069803	intronic	rs916134
Exon 2	C > G	chr12:54066271	intronic	rs10876480
	T > C	chr12:54066378	exonic (synonymous)	rs57929423
Exon 3	C > T	chr12:54063501	intronic	rs1800633
	A > G	chr12:54063493	intronic	rs1800634
	C > T	chr12:54063869	intronic	rs79533383
Exon 4	ins GTTTGTTT	chr12:54062799	intronic	–
Exon 5	ins. C	chr12:54059441	intronic	–
	C > T	chr12:54059281	intronic	rs71455254
ATPG3				
Exon 1	C > A	chr2:176046483	5′ UTR	–
	C > T	chr2:176046415	5′ UTR	rs268228
	C > T	chr2:176046408	5′ UTR	rs2217675
	C > A	chr2:176046392	5′ UTR	–
	ins. C	chr2:176046365	5′ UTR	–
	G > T	chr2:176046363	5′ UTR	rs147943553
	G > A	chr2:176046257	5′ UTR	rs268227
	G > T	chr2:176046167	5′ UTR	rs41270205
	G > A	chr2:176046007	intronic	rs73039765
Exon 3	A > T	chr2:176044136	intronic	rs268224
	C > A	chr2:176044008	intronic	rs12615406
	G > A	chr2:176043618	3′ UTR	rs268223
Exon 4	C > T	chr2:176042877	3′ UTR	rs189393963
	G > A	chr2:176042819	3′ UTR	rs2288960
	T > C	chr2:176043097	3′ UTR	rs8106

expressing ATP5G1^{WT}. To better understand the involvement of the ATP5G1^{G87E} mutation, two AC16 clones stably expressing both genotypes were established. In these cardiomyocytes, the altered PTPC channel activity promoted by ATP5G1^{G87E} led to decreased cell viability ($p < 0.0001$; Figure 2B) and increased propidium iodide (PI), Annexin V, and cleaved poly (ADP-ribose) polymerase (PARP) fluorescence intensity signals, as detected by using specific probes and antibodies in immunofluorescence analyses ($p < 0.01$; Figures 2C and 2D).

These findings reported directly from humans are further enhanced by the fact that Alavian et al. (2014) studied the impact of mutations in the glycine-rich domain of Csub on PTPC conductance and cell death. Mutational analysis involving the replacement of glycine with valine at this exact amino acid site (G87) allowed for the largest conductance of the pore and for increased oxidative-stress- and PTPC-dependent cell death compared to both the other three mutated glycines and ATP5G1^{WT}.

Because Csub is inevitably involved in both ATP synthesis and PTPC conductance (Norris et al., 1992), we performed an in-depth analysis on cell respiration and ATP synthesis by measuring the oxygen consumption rate (OCR) and mitochondrial ATP content by the Seahorse platform and the luciferin-luciferase assay (Morciano et al., 2017, 2020). First, we found a weak but significant decrease in the basal respiration rate in cells expressing ATP5G1^{G87E} compared to ATP5G1^{WT} (Figures 2E and 2F). In addition, we calculated the portion of respiration used to drive ATP synthesis, which was reduced in cells harboring Csub mutations (Figure 2F). Additionally, the mitochondrial ATP content was reduced (Figure 2G). Although these differences have been annotated, other mitochondrial parameters, including maximal respiration capacity (MRC), spare respiratory capacity, and remaining respiration not coupled to ATP

A

Gene	Variation	Functional position	Recurrence
ATP5G1	G>A (G87E)	Exon 3	2

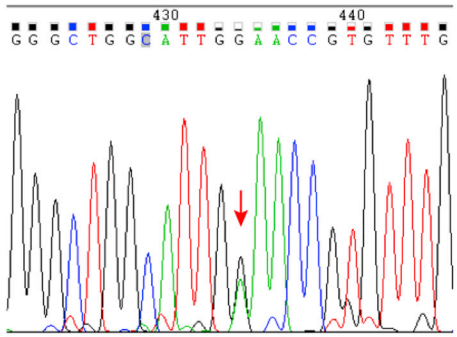

B

C

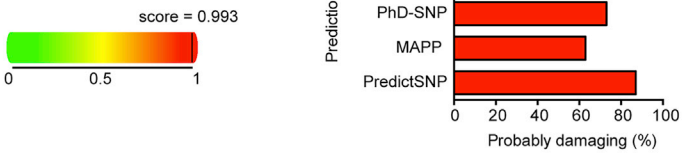

D

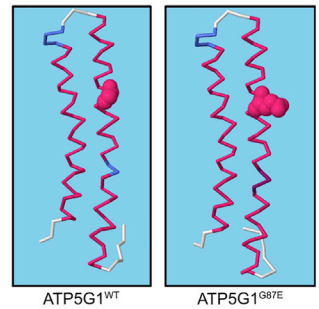

E

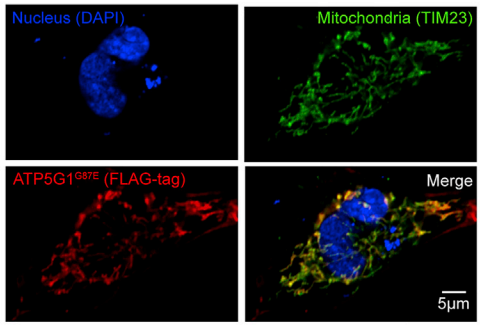

F

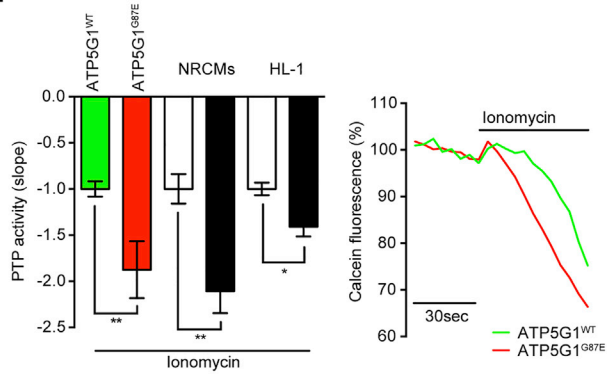

G

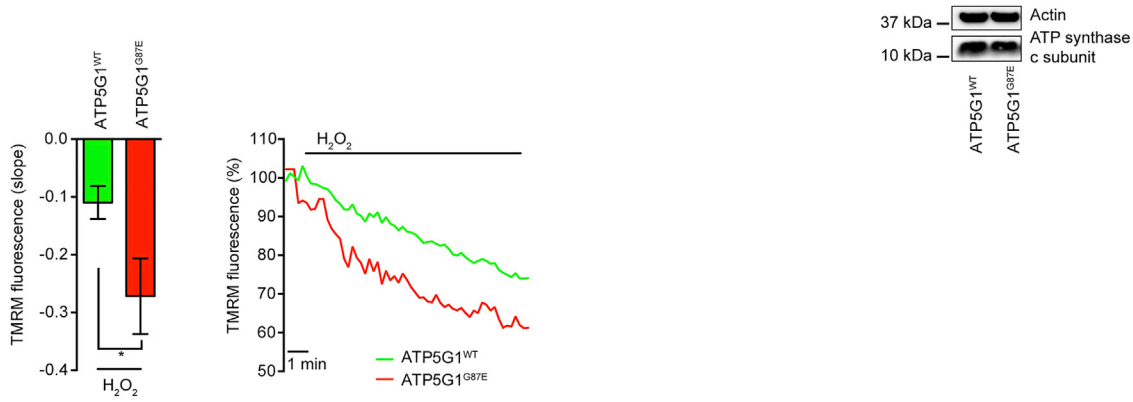

(legend on next page)

production, were unchanged. To understand whether changes in the expression of proteins involved in ATP synthesis occur, we then measured OXPHOS enzymes (Figure 2H) and those essential to the TCA cycle, namely, Aconitase1 and 2 (ACO1/2) and Citrate Synthase (CS) (Figure 2I); however, in this case, the levels remained unchanged.

With the aim of counteracting the deleterious effects of ATP5G1^{G87E} in H/R injury and to understand if these effects are dependent mainly on cell genotype and on PTPC activity, we repeated previous experiments in the presence of compound 10 (c.10), a selective Csub inhibitor known to have cardioprotective roles (Morciano et al., 2018). c.10 treatment desensitized channel activity, lowering the slope of the kinetics ($p < 0.05$ for ATP5G1^{WT} versus ATP5G1^{WT} + c.10 and for ATP5G1^{G87E} versus ATP5G1^{G87E} + c.10) (Figure 2J). Upon H/R, significantly more living cells were found in c.10-treated cells than in untreated cells ($p < 0.05$ for ATP5G1^{WT} versus ATP5G1^{WT} + c.10 and $p < 0.01$ for ATP5G1^{G87E} versus ATP5G1^{G87E} + c.10) with concomitant reduced PI and Annexin V staining (Figures 2K and 2L).

Taken together, these findings suggest that ATP5G1^{G87E} is involved in exacerbated PTPC-dependent H/R damage in human ventricular cardiomyocytes and that the genetic variation still responds to Csub inhibitors (Morciano et al., 2018) even when provided at the time of reperfusion. The fact that no differences were detected between ATP5G1^{WT} and ATP5G1^{G87E} under c.10 treatment (Figures 2K and 2L), this focuses solely on PTPC opening the exacerbated response to H/R rather than on the basal OCR variability (Figures 2E–2G).

To gain more insights into this naturally occurring mutation, we tried to enroll both patients bearing it. Unfortunately, one of them died as a consequence of MI, and from the remaining patient (named hereafter Id (identity) 24; male and 65 years old), we were unable to obtain cardiomyocytes for obvious reasons.

As the mutation is ubiquitously expressed, following written informed consent, we obtained fibroblasts by a 3-mm punch biopsy from the forearm of Id 24 and two age- and sex-matched volunteers (Id C1 and Id C2, not bearing the mutation). Functional analysis revealed strongly altered PTPC activity and mitochondrial membrane potential in the Id 24 sample (Figures 3A and 3B). This alteration was associated with decreased cell viability in Id 24 cells, as evaluated by PI uptake ($p < 0.001$ for Id C1 versus Id 24; $p < 0.0001$ for Id C2 versus Id 24) and crystal violet ($p < 0.05$ for Id C1 versus Id 24; $p < 0.01$ for Id C2 versus Id 24) approaches under H/R conditions (Figures 3C and 3D). Significantly greater PARP cleavage was also detected in Id 24 cells but not in control counterparts, as measured upon fluorescence detection and using a monoclonal specific antibody ($p < 0.01$ for Id C1 versus Id 24; $p < 0.001$ for Id C2 versus Id 24; Figure 3E).

Interestingly, in the absence of stressors (such as H/R), fibroblasts from healthy volunteers Id C1, Id C2, and Id 24 shared similar mitochondrial parameters in terms of morphology, mitochondrial membrane potential (Figures 3F and 3G), and mitochondrial and cytosolic Ca^{2+} handling (Figures S1A and S1B). The dimerization status of the ATP synthase complex was unchanged in the resting state (Figure S1D), and they exhibited similar expression levels of proteins that could be directly or indirectly involved in PTPC opening (Figure S1E).

Although Id 24 cells are characterized by a weak reduction in basal and ATP-linked respiration as well as maximal respiratory capacity (MRC) (Figures 3H and 3I) without variations in ACO1/2, SDHA, and CS proteins, as well as ATP5G1^{G87E}-expressing cardiomyocytes, these findings highlight once again a critical role of mutated Csub in PTPC opening only once H/R occurs.

The ATP5G1^{G87E}-dependent C-ring conformation is crucial for PTPC opening

To gain mechanistic insights into the role of ATP5G1^{G87E} in PTPC opening, we wondered whether protein stability was affected by the point mutation. We used three different kinds of assays to accurately address this issue. The first one, which was already established in Morciano et al. (2018), was a cellular thermal shift assay (CETSA) in which the degradation of Csub (detected by the use of the FLAG-tagged antibody) and MCU (as an inner membrane protein control) was quantified over time at increasing temperatures, from 53°C to 80°C. Figure 4A shows that the thermal-induced degradation of both ATP5G1^{WT} and ATP5G1^{G87E} proteins is statistically the same and does not differ from that of other inner mitochondrial membrane proteins, such as MCU. The second test was the detection of ubiquitin levels (Figure 4B), through which Csub is mainly degraded; and the third test, linked to the previous test, was the measure of proteasome activity (Figure 4C). The independent results obtained in all

Figure 1. ATP5G1^{G87E} is predicted to be damaging and alters PTPC activity in human ventricular cardiomyocytes

(A) The genetic profile of ATP5G1^{G87E} variation (left) and capillary electrophoresis of the DNA sequencing of the two patients carrying the mutation (right); arrow indicates the presence of the variation in heterozygosis.

(B) Csub coding sequence alignment among different species. the glycine-rich region is highlighted by four red rectangles, and the arrow indicates the site of amino acid substitution.

(C) Data output from PolyPhen 2 software (on the left) in which green indicates the probability of a benign variation and red indicates damage. The black line indicates the score predicted by the software. The outputs of the other six different predictive software programs (y axis) are shown on the right, where red indicates that the variation is damaging, and their probability is shown on the x axis.

(D) The output of RaptorX software highlighting the steric hindrance of the amino acid substitution.

(E) Expression and colocalization of ATP5G1^{G87E} mutated protein (in red, by an anti-FLAG antibody as a tag of the plasmid) with the mitochondrial network detected by the TIM23 antibody seen in the AC16 cell line. Scale bar, 5 μm

(F) Calcein-cobalt quenching assay of AC16 cells, neonatal rat cardiomyocytes (NRCMs; white bar for ATP5G1^{WT} and black bar for ATP5G1^{G87E}), and HL-1 cells (white bar for ATP5G1^{WT} and black bar for ATP5G1^{G87E}), for which PTPC activity is reported as the slope of the kinetics following ionomycin (500 nM) administration. A western blot (WB) is presented in this panel to show the same expression of Csub in both experimental conditions of this paper.

(G) Mitochondrial membrane potential in AC16 cells using the TMRM probe reported as the slope of the kinetics following hydrogen peroxide (500 μM) administration.

At least 18 cells per independent working day (n = 4) were evaluated for microscopic analysis. All histograms report means with SEM. *: p value < 0.05; **: p value < 0.01.

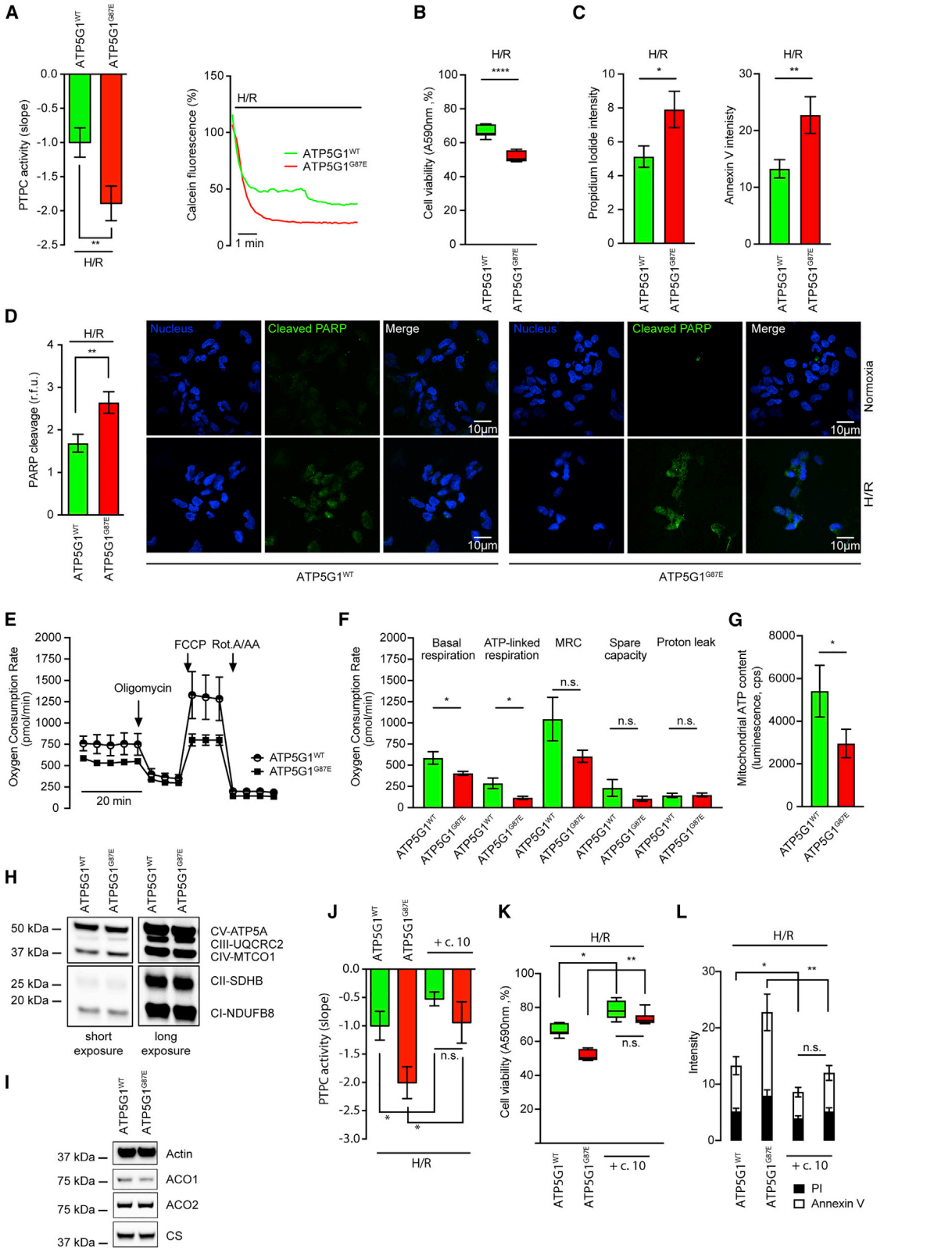

(legend on next page)

three assays demonstrated how the mutation does not affect protein stability.

As explored in fibroblasts from patients (Figure S1D), WT and mutated AC16 cells expressed the same ratio of dimers (Figure 4D), reflecting no differences in PTPC opening at resting state due to variation in the ratio of dimers-monomers.

Recently, we published the multistep nature of PTPC formation, which first involves the destabilization of dimers of ATP synthase, followed by a given C-ring conformation-dependent activity of the pore (Bonora et al., 2017). Now, with the same purpose, we wondered whether the ATP5G1^{G87E} mutation triggers the opening of the PTPC, secondarily to dimer disassembly and dependently on its acquired conformation, which, predictively, differs from the WT conformation. Overexpression of ATPIF1 in ATP5G1^{WT} and ATP5G1^{G87E} cells, which is known to increase the amount of ATP synthase dimers and induce strong PTPC desensitization (Bonora et al., 2017), significantly alleviates differences in PTPC opening between conditions under mitochondrial Ca^{2+} overload (Figure 4E). Likewise, destabilization of ATP synthase dimers by ATP5I silencing (a protein involved in dimer stabilization; Bonora et al., 2017) triggers an abrupt increase in PTPC conductance, which is greater in ATP5G1^{G87E} cells (Figure 4F). Taken together, these findings highlight a role for the predicted conformational change of the mutated C-ring, second to F_1F_O-ATP synthase dimer disassembly.

The latest findings reported that the final step of PTPC gating would involve F_1 portion detachment (Pinke et al., 2020). We wanted to check this in mitochondria isolated from cardiomyocytes under our experimental conditions, and we wondered whether the ATP5G1^{G87E} mutation may further influence F_1 detachment compared to Csub WT overexpression, allowing for the abrupt increase in PTPC opening. Thus, we explored the expression of proteins composing the F_1 portion and Csub with and without ionomycin treatment. Triggering PTPC opening, we found a decrease in the expression of ATP5A, ATP5B, and OSCP F_1 proteins but not in the levels of Csub (Figure 4G). No additional differences between ATP5G1^{WT} and ATP5G1^{G87E} were detected.

Because it has been reported that a structural and functional interaction occurs between Csub and MCU (Huang and Docampo, 2020), which allows for ATP-synthase-conserving properties and that the glycine-rich domain plays a key role in this interaction, we investigated whether changes in intracellular Ca^{2+} fluxes occur in the presence of mutated Csub. However, our data revealed no changes in terms of basal and stimulated mitochondrial and cytosolic Ca^{2+} (Figures 4H–4L).

PTPC activity is significantly related to RI in STEMI patients

As validated by multiple studies (Bononi et al., 2017; Chakrabarty et al., 2017; Jimenez-Mallebrera et al., 2006; Mak et al., 2011), skin-biopsy-derived fibroblasts can be used for functional analyses in multiple disease settings, especially when obtaining specific biopsy specimens is not possible. Indeed, processing heart samples or myocytes for research purposes is challenging, even considering the continual development of semi-invasive or percutaneous procedures in the treatment of acute infarction.

Thus, with the aim of understanding whether PTPC activity can change among individuals and whether pore opening is significantly related to RI, we conducted a pilot study in a cohort of 14 patients with anterior MI undergoing PCI (Table S3). In this setting, skin biopsies from the forearm of patients were used to obtain fibroblasts for functional tests (Figures 5A and 5B). Cardiac magnetic resonance imaging (cMRI) was performed to assess reperfusion damage (Figure 5C). By measuring PTPC opening in fibroblasts from each STEMI patient, as evaluated by both calcein-cobalt and tetramethylrhodamine, methyl ester, perchlorate (TMRM) techniques under Ca^{2+}- and ROS-dependent conditions, we found intersubject variability in the PTPC activity of STEMI patients. We also observed a significant correlation of the myocardial salvage index (MSI) with PTPC activity (Spearman's R = 0.79, p = 0.001) and mitochondrial membrane potential (Spearman's R = 0.71, p = 0.006) (Figure 5D). However, and importantly, there were no significant differences in the baseline characteristics of the patients stratified according to the median MSI value (0.44; Table S3). None of the variables listed in Table S3 were related to PTPC activity or mitochondrial membrane potential values. Overall, patients with greater reperfusion damage (an MSI below the median value) exhibited significantly higher PTPC activity and mitochondrial membrane

Figure 2. ATP5G1^{G87E} variation exacerbates H/R-dependent cell damage in human ventricular cardiomyocytes

(A) Calcein-cobalt quenching assay in AC16 cells at the time of reperfusion in a hypoxic chamber, for which PTPC activity is reported as the slope of the kinetics.

(B) Quantification of cell viability in AC16 clones stably expressing ATP5G1^{WT} and ATP5G1^{G87E} under I/R conditions. The results are reported as percentages.

(C) Quantification of PI and Annexin V staining in AC16 cells under the same conditions as in (B).

(D) Cleaved PARP immunofluorescence detection and quantification by confocal microscopy in AC16 clones stably expressing ATP5G1^{WT} and ATP5G1^{G87E}; the statistics and representative images under normoxia and I/R are reported. The results are reported as relative fluorescence units (r.f.u.s). Scale bar, 10 μm.

(E) Oxygen consumption rate (OCR) kinetics reporting mean values with standard errors of all experiments done.

(F) Analysis of OCR over time with statistics following stimulus addition for the calculation of basal respiration rate, ATP-linked respiration, maximal respiratory capacity (MRC), spare capacity, and proton leakage.

(G) Mitochondrial ATP content measured by luciferin-luciferase assay; cps, counts per second.

(H) Detection of OXPHOS enzyme expression by WB analysis; short and long exposure of the five complexes of the electron transport chain.

(I) Detection of mitochondrial enzymes crucial for the TCA cycle and ATP synthesis, namely, Aconitase 1 and 2 (ACO1/2) and Citrate Synthase (CS).

(J) Calcein-cobalt quenching assay in AC16 clones stably expressing ATP5G1 WT and ATP5G1^{G87E}, for which PTPC activity is reported as the slope of the kinetics at the time of reoxygenation after ischemia with and without the Csub inhibitor compound 10 (c.10).

(K) Quantification of cell viability under the same conditions as in (J). The results are reported as percentages.

(L) PI and Annexin V staining quantification in AC16 cells under the same conditions as in (K).

At least 18 cells per independent working day (n = 4) were evaluated for microscopic analysis. At least 2 replicates for n = 3 independent working days for cell death and cell viability assays. At least 5 replicates for n = 2 independent working days for OXPHOS and ATP measures. At least 3 replicates for WB analysis. All graphs report means with SEM. For statistics, please refer to Results and STAR methods. *: p value < 0.05; **: p value < 0.01.

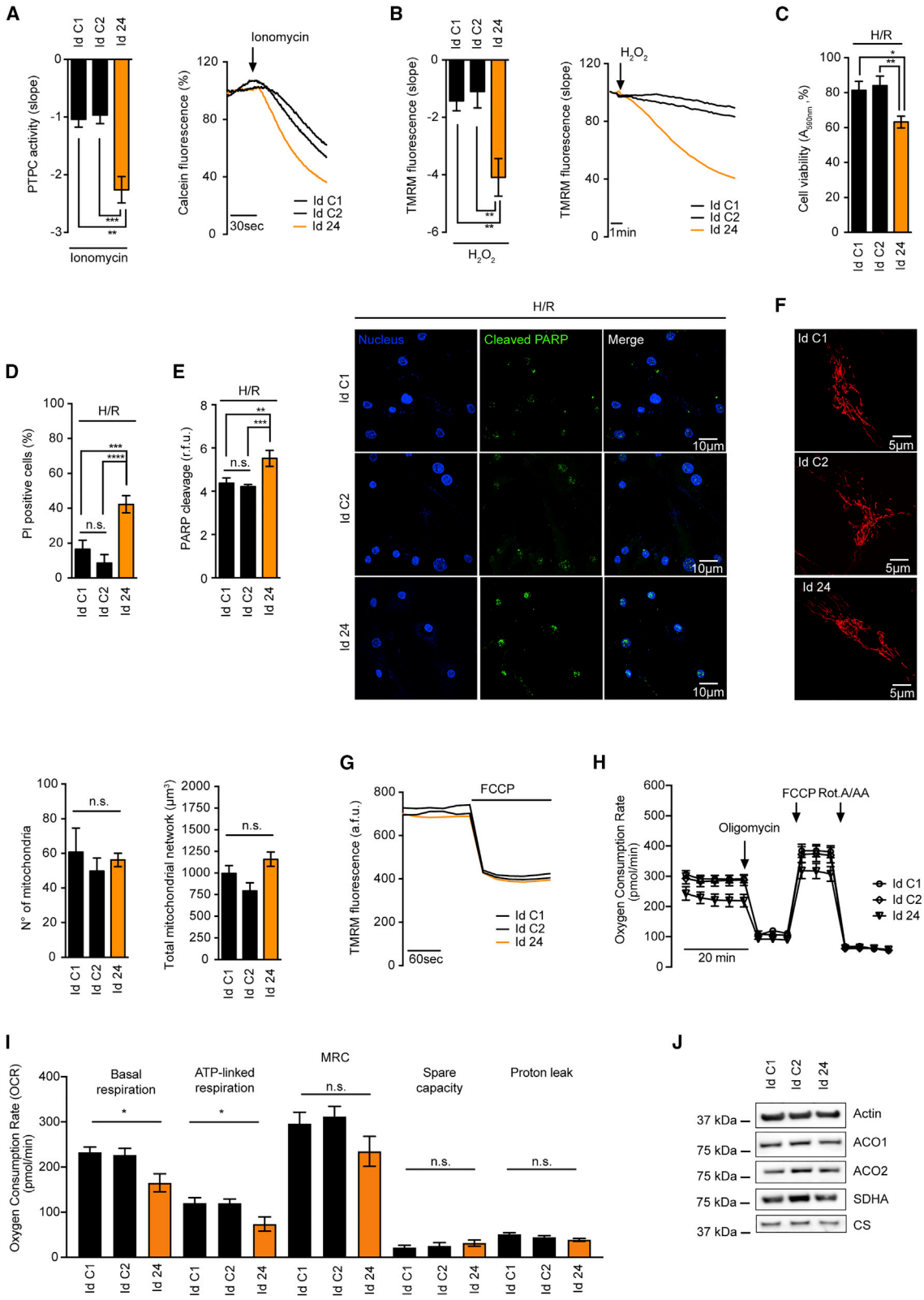

(legend on next page)

potential values than other patients (Figure 5E). Figure 5F shows representative cMRI images between two STEMI patients; ID3 experienced hyperresponsive opening of the PTPC and exhibited a final infarct size (IS) of 26%, and the ID12 was subjected to hyporesponsive PTPC opening and exhibited a final IS of 7%. Taken together, these data suggest an interesting relationship between PTPC activity and reperfusion damage in patients.

DISCUSSION

To the best of our knowledge, there is no translational data linking either PTPC opening with myocardial salvage induced by primary angioplasty in patients with STEMI or genetic determinants of PTPC with H/R-dependent damage *in vitro*. This knowledge gap is related, on the one hand, to the difficulty of assessing the variation of PTPC function of ischemic/reperfused patients and, on the other hand, to the concomitant effect of reperfusion on recovery of contractile function. This is relevant to establish whether, as suggested from animal experimental data, the opening of the PTPC is responsible for incomplete recovery of contractile function on reperfusion in human patients and, consequently, whether the modulation of components, particularly Csub, could be considered therapeutically. This last aspect has also been investigated by Shanmuganathan et al. (2005), who suggested that CsA-mediated PTPC inhibition directly in atrial tissue is a valuable tool for cardioprotection.

Given this background, we sequenced all three Csub-encoding genes in a cohort of STEMI patients in which we detected the ATP5G1^{G87E} variant, a heterozygous missense mutation found in exon 3 of the *ATP5G1* gene, in two individuals (Table 1; Figure 1). This mutated glycine is part of a glycine-rich and highly conserved domain of Csub (Figure 1; Norris et al., 1992); it has been reported that modifications at this site determine the loss of structural and functional MCU-Csub interaction (G87L replacement) (Huang and Docampo, 2020) and C-ring conformational changes that significantly impact the conductance of the channel and PTPC-mediated cell death (G87V replacement) (Alavian et al., 2014).

As expected, *in silico* approaches using the highly established predictive software PolyPhen 2 classified the ATP5G1^{G87E} variant as probably damaging once expressed. This notion has been confirmed by six additional software programs (Figure 1) and *in vitro* by a series of functional analyses following H/R conditions performed in both human cardiomyocytes and fibroblasts from one of the two STEMI patients carrying the mutation. Indeed, H/R led to a significant decrease in the viability of cells expressing ATP5G1^{G87E} compared with their control counterparts (Figures 2 and 3).

Although cells expressing mutations show a reduced basal respiration rate, ATP-linked respiration, and ATP mitochondrial content, these variations in H/R damage are only secondary to an exacerbated PTPC opening because treatment with c.10 at reoxygenation time, a selective PTPC inhibitor, mitigated the deleterious effects of the Csub mutated form, similar to the WT. In addition, because we failed to demonstrate further differences in mitochondrial parameters in the absence of stressors (such as H/R), we speculated that the ATP5G1^{G87E} variant would be deleterious only at reperfusion time, once MI has developed, and would be the main culprit of exacerbated damage. These findings indirectly suggest that the harmful effects brought about by reperfusion in the 2 out of 52 patients with the mutation could indeed be dependent on the expression of the ATP5G1^{G87E} genotype and that the use of Csub inhibitors at the time of reperfusion could be therapeutically useful.

Very recently, cryoelectron microscopy revealed an atomic model of ovine F_1F_O-ATP synthase describing, in a detailed pathway, what happens when Ca^{2+} overload occurs in mitochondria. Under PTPC opening conditions, the retraction of subunit e and changes in the C-ring conformation have been reported, yet once again validating our hypothesis and findings; the F_1 portion detachment is proposed as the final step of a mechanism allowing full conductance of the pore (Pinke et al., 2020). To investigate this in cardiomyocytes and following our experimental conditions, we triggered PTPC opening by inducing Ca overload in ATP5G1^{WT}- and ATP5G1^{G87E}-overexpressing cells. Although we reported a decrease in F_1 proteins upon ionomycin treatment, suggesting

Figure 3. Analysis of PTPC-mediated deleterious effects in cells from patients carrying mutations

(A) Calcein-cobalt quenching assay of fibroblasts from skin biopsies of the STEMI patient carrying the mutation (Id 24, orange bar) and control counterparts (Id C1 and Id C2, black bars). PTPC activity is reported as the slope of the kinetics following ionomycin administration (500 nM).

(B) Mitochondrial membrane potential in the same cells of (A) by a TMRM assay reported as the slope of the kinetics following hydrogen peroxide administration (500 μM).

(C and D) Quantification of cell viability (C) according to cells that remained alive upon H/R staining with crystal violet and with incorporated PI (D). The results are reported as percentages.

(E) Cleaved PARP detection and quantification by immunofluorescence in confocal microscopy; statistics and representative images under H/R are reported. The results are represented as r.f.u.s. Scale bar, 10 μm.

(F) Mitochondrial morphology in Id C1, Id C2, and Id 24 cells analyzed by MitoTracker Deep Red and confocal microscopy. Representative images are shown on the top, and statistics regarding the number of mitochondria and their total mitochondrial network (y axis) are shown on the bottom. Scale bar, 5 μm.

(G) Basal mitochondrial membrane potential analyzed by the TMRM probe and fluorescence microscopy.

(H) OCR kinetics reporting mean values with standard errors of all experiments performed.

(I) Analysis of OCR over time with statistics following stimuli addition for calculation of basal respiration rate, ATP-linked respiration, MRC, spare capacity, and proton leak.

(J) Detection of mitochondrial enzymes crucial for the TCA cycle and ATP synthesis, namely, ACO1/2, CS, and Succinate Dehydrogenase Complex Flavoprotein Subunit A (SDHA). At least 16 cells per independent working day (n = 4) were evaluated for microscopic analysis.

At least 2 replicates for n = 3 independent working days for cell death and cell viability assays. At least 5 replicates for n = 2 independent working days for OXPHOS and ATP measures. At least 2 replicates for WB analysis. All graphs report means with SEM. For statistics, please refer to Results and STAR methods. *: p value < 0.05; **: p value < 0.01; ***: p value < 0.001; ****: p value < 0.0001.

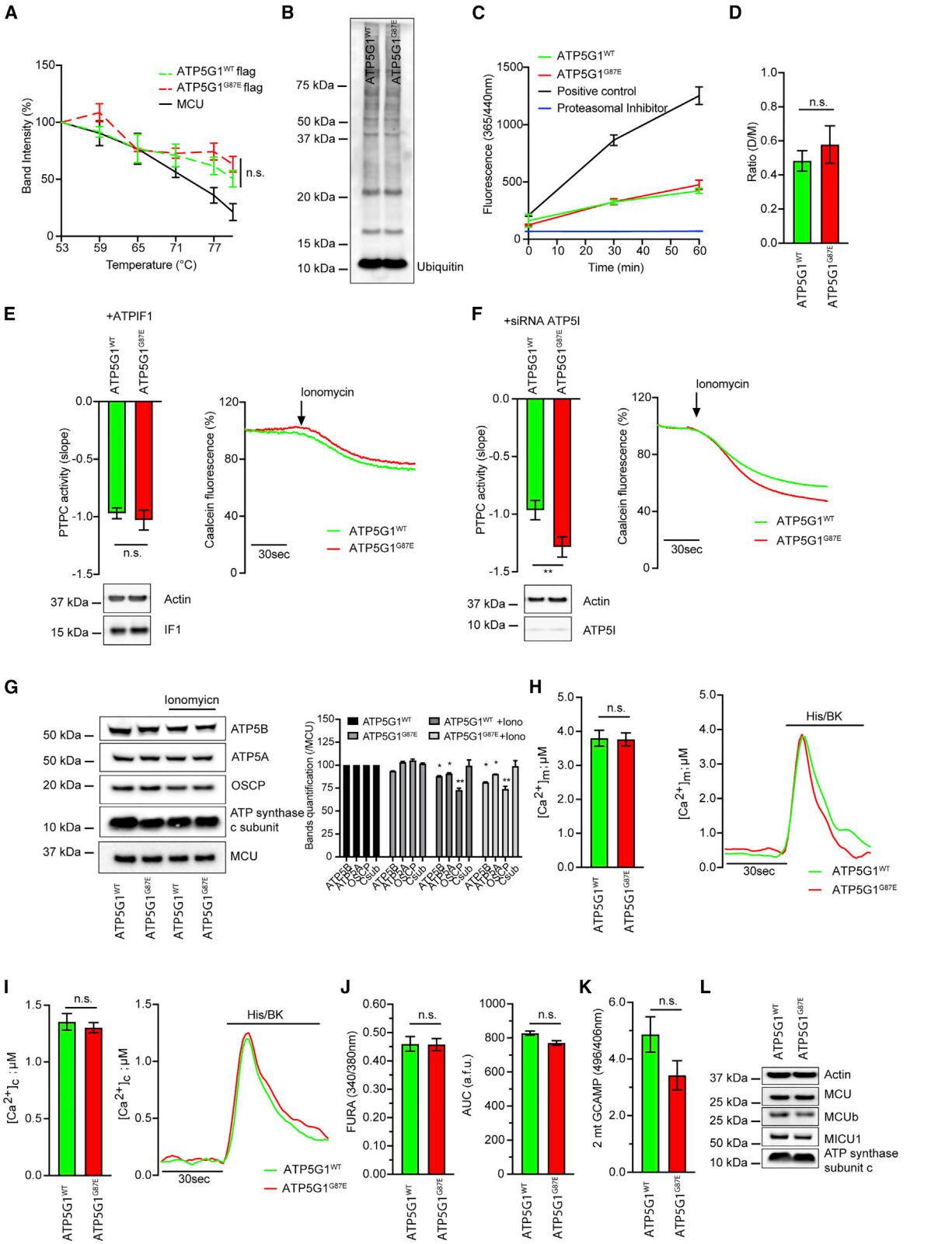

(legend on next page)

changes in F_1-F_O stoichiometry in favor of the greatest amount of Csub available to pore opening, no differences were detected between experimental conditions. This result further supports the hypothesis that what truly changes in the presence of the G87E amino acid substitution is the conformational change at the C-ring level. Further research involving Csub knockout (KO) and ATP5G1^{G87E} knockin (KI) cells is needed to confirm the latter result.

Although our line of research shares great findings about the MCU-Csub interaction and may partially explain the reduced OCR and mitochondrial ATP content in cells expressing ATP5G1^{G87E}, our data on intracellular Ca^{2+} fluxes and proteins involved in its handling tend to exclude this hypothesis in this pathological context.

It should be noted that fibroblasts have often been used as models for other cell types in pathological contexts in which a given biopsy specimen (in our case, ventricular cardiomyocytes) cannot be collected (Bononi et al., 2017; Chakrabarty et al., 2017; Jimenez-Mallebrera et al., 2006; Mak et al., 2011).

To understand whether variability in PTPC activity exists among STEMI patients, even in the absence of mutations, and whether this variability may be linked to RI, we performed a pilot study in 14 patients selected for having a lesion of the left anterior descending (LAD) coronary artery. First, we found a significant variability in PTPC opening in the cohort of patients and, second, a direct correlation with a strong statistical significance between the opening of the PTPC and the reperfusion damage developed upon PCI (Figure 5). Patients with lower MSI (and therefore larger reperfusion damage) showed the highest value of fibroblast PTPC activity and mitochondrial membrane potential (Figure 5). These findings suggest that some patients could be more predisposed than others to reperfusion injury (RI).

We recognize that this study contains limitations regarding the small cohorts of patients analyzed. Our idea was to improve current knowledge about the PTPC in I/R injury in human patients, which would be useful for planning possible targeted individualized pharmacological approaches to be tested in properly sized clinical trials.

STAR★METHODS

Detailed methods are provided in the online version of this paper and include the following:

- KEY RESOURCES TABLE
- RESOURCE AVAILABILITY
  - Lead contact
  - Materials availability
  - Data and code availability
- EXPERIMENTAL MODEL AND SUBJECT DETAILS
  - AC16 and fibroblasts cells
  - STEMI patients
- METHOD DETAILS
  - C subunit genetic screening
  - Blood sample collection
  - DNA extraction
  - PCR amplification, sequencing and analysis
  - Predictive software
  - Cell culture and transient transfection
  - Hypoxia/reoxygenation protocol
  - PTPC measurements
  - Basal mitochondrial membrane potential
  - Mitochondrial morphology
  - Immunofluorescence
  - Annexin-V and Propidium iodide assays
  - Ca^{2+} measurements
  - Proximity ligation assay (PLA)
  - Immunoblot analysis
  - Cell viability assay (Crystal violet)
  - Oxygen Consumption Rate
  - Luciferine-luciferase assay
  - Cellular Thermal Shift Assay (CETSA)
  - Proteasome activity assay kit
  - Blue-native PAGE and in gel activity assay
  - Analysis of F_1-ATP synthase proteins
  - Study population for PTPC function and reperfusion damage tests and C subunit genetic screening

Figure 4. ATP5G1^{G87E}-dependent C-ring conformation alters PTPC opening

(A) Cellular thermal shift assay (CETSA) in AC16 cells expressing ATP5G1^{WT} or ATP5G1^{G87E}. Kinetics (mean values with standard error) representing the degradation of the proteins of interest over time due to increased temperature from 53°C to 80°C. Values derive from band quantification of WB. Under both conditions, the degradation of two proteins was measured, namely, FLAG-tag Csub and MCU, black line, as an internal control.

(B) WB to detect protein ubiquitination.

(C) Proteasomal activity assay in AC16 cells under both experimental conditions, following the manufacturer's instructions.

(D) ATP synthase dimer/monomer ratio in AC16 cells expressing ATP5G1^{WT} or ATP5G1^{G87E} evaluated with blue-native PAGE followed by gel activity assay.

(E) Calcein-cobalt quenching assay in AC16 cells expressing ATP5G1^{WT} or ATP5G1^{G87E} and overexpressing ATPIF1 following ionomycin administration, for which PTPC activity is reported as the slope of the kinetics. WB was included to assess equal ATPIF1 overexpression.

(F) Calcein-cobalt quenching assay in AC16 cells expressing ATP5G1^{WT} or ATP5G1^{G87E} and silenced for ATP5I following ionomycin administration, for which PTPC activity is reported as the slope of the kinetics. WB is included to assess equal ATP5I silencing.

(G) Expression of F_1-portion proteins and Csub in ATP5G1^{WT} and ATP5G1^{G87E} AC16 cells before and after prompting PTPC opening by ionomycin addition.

(H) Mitochondrial Ca^{2+} uptake in AC16 cells upon stimulus (histamine/bradykinin) administration.

(I) Cytosolic Ca^{2+} flux in AC16 cells upon stimulus (histamine/bradykinin) administration.

(J) Analysis of FURA experiments highlighting basal cytosolic Ca^{2+} (on the left) and Ca^{2+} release into the cytosol (on the right). The area under the curve (AUC) is the area calculated under the peak generated by Ca^{2+} flux upon stimulus.

(K) Analysis of basal mitochondrial Ca^{2+} by the use of the 2 mt-GCAMP plasmid.

(L) Expression of the main proteins involved in mitochondrial Ca^{2+} handling. n.s., not significant.

At least 16 cells per independent working day (n = 4) were evaluated for microscopic analysis; at least 12 cells per independent working day (n = 3) for Ca^{2+} measurements; at least 2 replicates for WB analysis; at least 2 replicates per independent working day (n = 2) for the proteasome assay. All graphs report means with SEM. *: p value < 0.05; **: p value < 0.01.

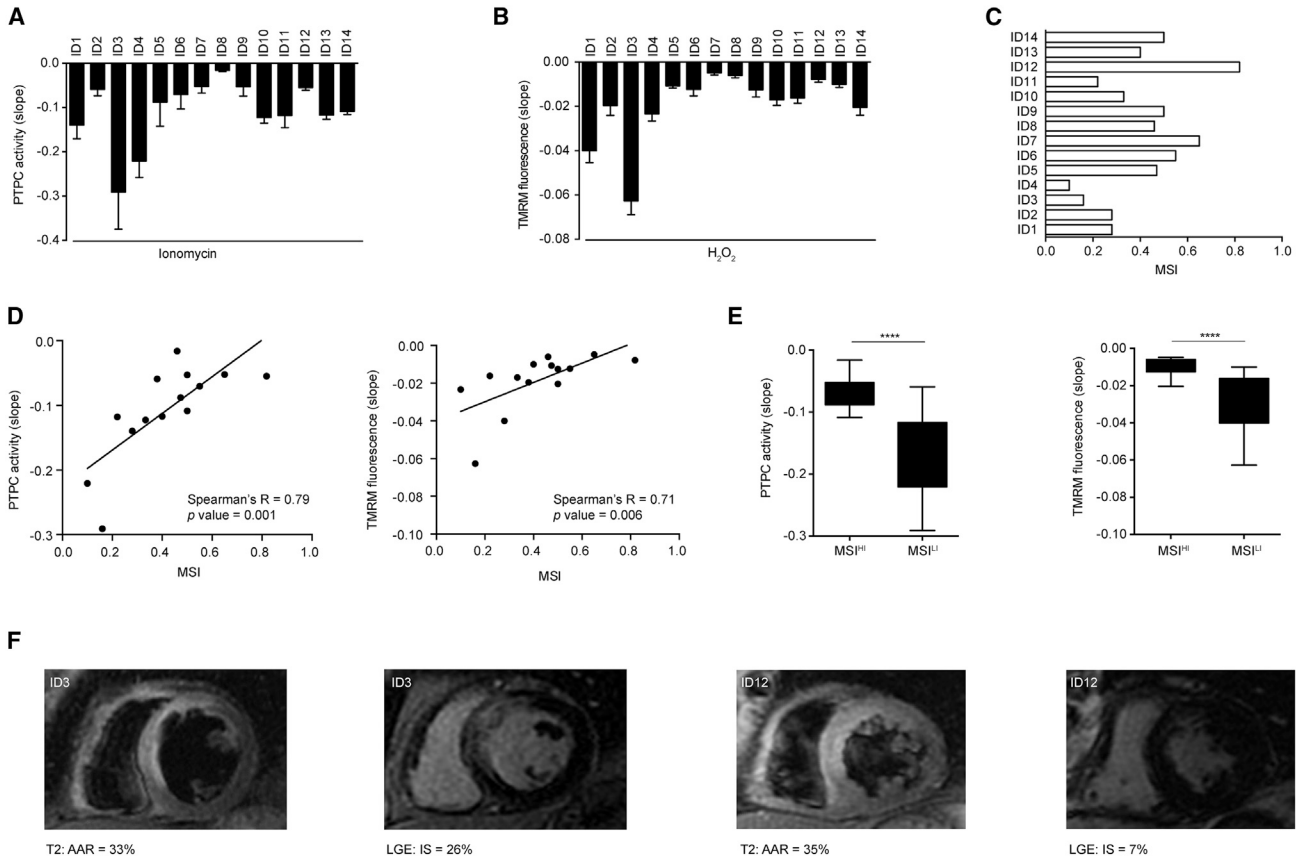

Figure 5. Correlation between PTPC function and reperfusion damage in STEMI patients

(A) The calcein-cobalt quenching assay of fibroblasts from skin biopsies of STEMI patients. PTPC activity is reported as the slope of the kinetics following ionomycin administration (500 nM), as indicated.

(B) Mitochondrial membrane potential in the same cells of (A) by a TMRM assay reported as the slope of the kinetics following hydrogen peroxide administration (500 μM), as indicated.

(C) MSI from cMRI.

(D) Graphs depicting the correlation between PTPC activity and MSI (on the left) and between mitochondrial membrane potential and MSI (on the right) measured in fibroblasts from STEMI patients. Spearman's R and p values are reported.

(E) Stratification of PTPC and mitochondrial membrane potential values according to the median MSI value.

(F) Representative cMRI images for the two STEMI patients, namely, ID12 with hyporesponsive PTPC opening and limited IS (7%) and ID3 with hyperresponsive PTPC opening and extensive IS (26%).

At least 16 cells per independent working day (n = 4) were evaluated for microscopic analysis. All graphs report means with SEM. For statistics, please refer to Results and STAR methods. "****: p value < 0.0001.

- ○ Skin biopsy
- ○ Cardiac MRI

● QUANTIFICATION AND STATISTICAL ANALYSIS

SUPPLEMENTAL INFORMATION

Supplemental information can be found online at https://doi.org/10.1016/j.celrep.2021.108983.

ACKNOWLEDGMENTS

P.P. is grateful to Camilla degli Scrovegni for continuous support. The Signal Transduction Laboratory (http://sm.unife.it/it/ricerca-e-terza-missione/ricerca-1/ambiti/signaltransductionlab/labPP) is supported by the Italian Association for Cancer Research (AIRC: IG-23670 to P.P. and IG-19803 to C.G.), A-ROSE, Telethon (GGP11139B to P.P.), Progetti di Rilevante Interesse Nazionale (PRIN2017E5 L5P3 to P.P. and PRIN20177E9EPY to C.G.), the Italian Ministry of Health (GR-2013-02356747 to C.G.), the European Research Council (ERC; 853057-InflaPML to C.G.), and local funds from the University of Ferrara to P.P. and C.G.; M.R.W. and M.L.-A. were supported by the Polish National Science Centre (grant UMO-2014/15/B/NZ1/00490). G.M. is grateful to Pierangelo M. for his support.

AUTHOR CONTRIBUTIONS

G.M. conceived, planned, and wrote the manuscript; performed the experiments; and conceived figures. G.P. performed the experiments; M.L.-A. evaluated the monomeric/dimeric state of ATP synthase; M.B. and L.G. corrected the manuscript; R.P. and G.C. managed clinical parts of study B; E.M., S.C., and A.A. managed clinical parts of study A; M.B. and M.P. managed genetic investigations of study C; M.R.W. and C.G. helped to refine the draft from a biochemical point of view; R.F. helped to refine the

draft from a clinical point of view; and P.P. conceived and corrected the manuscript.

DECLARATION OF INTERESTS

There are no competing interests.

Received: August 24, 2020
Revised: February 7, 2021
Accepted: March 22, 2021
Published: April 13, 2021

REFERENCES

Adzhubei, I., Jordan, D.M., and Sunyaev, S.R. (2013). Predicting functional effect of human missense mutations using PolyPhen-2. Curr. Protoc. Hum. Genet. *Chapter 7*, Unit 7.20.

Alavian, K.N., Beutner, G., Lazrove, E., Sacchetti, S., Park, H.A., Licznerski, P., Li, H., Nabili, P., Hockensmith, K., Graham, M., et al. (2014). An uncoupling channel within the c-subunit ring of the F1FO ATP synthase is the mitochondrial permeability transition pore. Proc. Natl. Acad. Sci. USA *111*, 10580–10585.

Azarashvili, T., Odinokova, I., Bakunts, A., Ternovsky, V., Krestinina, O., Tyynelä, J., and Saris, N.E. (2014). Potential role of subunit c of F0F1-ATPase and subunit c of storage body in the mitochondrial permeability transition. Effect of the phosphorylation status of subunit c on pore opening. Cell Calcium *55*, 69–77.

Bononi, A., Giorgi, C., Patergnani, S., Larson, D., Verbruggen, K., Tanji, M., Pellegrini, L., Signorato, V., Olivetto, F., Pastorino, S., et al. (2017). BAP1 regulates IP3R3-mediated Ca^{2+} flux to mitochondria suppressing cell transformation. Nature *546*, 549–553.

Bonora, M., Bononi, A., De Marchi, E., Giorgi, C., Lebiedzinska, M., Marchi, S., Patergnani, S., Rimessi, A., Suski, J.M., Wojtala, A., et al. (2013a). Role of the c subunit of the FO ATP synthase in mitochondrial permeability transition. Cell Cycle *12*, 674–683.

Bonora, M., Giorgi, C., Bononi, A., Marchi, S., Patergnani, S., Rimessi, A., Rizzuto, R., and Pinton, P. (2013b). Subcellular calcium measurements in mammalian cells using jellyfish photoprotein aequorin-based probes. Nat. Protoc. *8*, 2105–2118.

Bonora, M., Morganti, C., Morciano, G., Giorgi, C., Wieckowski, M.R., and Pinton, P. (2016). Comprehensive analysis of mitochondrial permeability transition pore activity in living cells using fluorescence-imaging-based techniques. Nat. Protoc. *11*, 1067–1080.

Bonora, M., Morganti, C., Morciano, G., Pedriali, G., Lebiedzinska-Arciszewska, M., Aquila, G., Giorgi, C., Rizzo, P., Campo, G., Ferrari, R., et al. (2017). Mitochondrial permeability transition involves dissociation of F_1F_O ATP synthase dimers and C-ring conformation. EMBO Rep. *18*, 1077–1089.

Bonora, M., Wieckowski, M.R., Sinclair, D.A., Kroemer, G., Pinton, P., and Galluzzi, L. (2019). Targeting mitochondria for cardiovascular disorders: therapeutic potential and obstacles. Nat. Rev. Cardiol. *16*, 33–55.

Campo, G., Morciano, G., Pavasini, R., Bonora, M., Sbano, L., Biscaglia, S., Bovolenta, M., Pinotti, M., Punzetti, S., Rizzo, P., et al. (2016). Fo ATP synthase C subunit serum levels in patients with ST-segment Elevation Myocardial Infarction: Preliminary findings. Int. J. Cardiol. *221*, 993–997.

Campo, G., Pavasini, R., Morciano, G., Lincoff, A.M., Gibson, C.M., Kitakaze, M., Lonborg, J., Ahluwalia, A., Ishii, H., Frenneaux, M., et al. (2017a). Clinical benefit of drugs targeting mitochondrial function as an adjunct to reperfusion in ST-segment elevation myocardial infarction: A meta-analysis of randomized clinical trials. Int. J. Cardiol. *244*, 59–66.

Campo, G., Pavasini, R., Morciano, G., Lincoff, M.A., C Gibson, M., Kitakaze, M., Lonborg, J., Ahluwalia, A., Ishii, H., Frenneaux, M., et al. (2017b). Data on administration of cyclosporine, nicorandil, metoprolol on reperfusion related outcomes in ST-segment Elevation Myocardial Infarction treated with percutaneous coronary intervention. Data Brief *14*, 197–205.

Chakrabarty, B., Sharma, M.C., Gulati, S., and Sarkar, C. (2017). Skin Biopsy for Diagnosis of Ullrich Congenital Muscular Dystrophy: An Observational Study. J. Child Neurol. *32*, 1099–1103.

Chinopoulos, C. (2017). ATP synthase complex and the mitochondrial permeability transition pore: poles of attraction. EMBO Rep. *18*, 1041–1042.

Chinopoulos, C., and Adam-Vizi, V. (2012). Modulation of the mitochondrial permeability transition by cyclophilin D: moving closer to F(0)-F(1) ATP synthase? Mitochondrion *12*, 41–45.

Cung, T.T., Morel, O., Cayla, G., Rioufol, G., Garcia-Dorado, D., Angoulvant, D., Bonnefoy-Cudraz, E., Guérin, P., Elbaz, M., Delarche, N., et al. (2015). Cyclosporine before PCI in Patients with Acute Myocardial Infarction. N. Engl. J. Med. *373*, 1021–1031.

Eitel, I., Desch, S., Fuernau, G., Hildebrand, L., Gutberlet, M., Schuler, G., and Thiele, H. (2010). Prognostic significance and determinants of myocardial salvage assessed by cardiovascular magnetic resonance in acute reperfused myocardial infarction. J. Am. Coll. Cardiol. *55*, 2470–2479.

Elustondo, P.A., Nichols, M., Negoda, A., Thirumaran, A., Zakharian, E., Robertson, G.S., and Pavlov, E.V. (2016). Mitochondrial permeability transition pore induction is linked to formation of the complex of ATPase C-subunit, polyhydroxybutyrate and inorganic polyphosphate. Cell Death Discov. *2*, 16070.

Ferrari, R., Balla, C., Malagù, M., Guardigli, G., Morciano, G., Bertini, M., Biscaglia, S., and Campo, G. (2017). Reperfusion Damage—A Story of Success, Failure, and Hope. Circ. J. *81*, 131–141.

Giorgi, C., Marchi, S., and Pinton, P. (2018). The machineries, regulation and cellular functions of mitochondrial calcium. Nat. Rev. Mol. Cell Biol. *19*, 713–730.

Griffiths, E.J., and Halestrap, A.P. (1995). Mitochondrial non-specific pores remain closed during cardiac ischaemia, but open upon reperfusion. Biochem. J. *307*, 93–98.

Huang, G., and Docampo, R. (2020). The Mitochondrial Calcium Uniporter Interacts with Subunit c of the ATP Synthase of Trypanosomes and Humans. mBio *11*, e00268-20.

Jimenez-Mallebrera, C., Maioli, M.A., Kim, J., Brown, S.C., Feng, L., Lampe, A.K., Bushby, K., Hicks, D., Flanigan, K.M., Bonnemann, C., et al. (2006). A comparative analysis of collagen VI production in muscle, skin and fibroblasts from 14 Ullrich congenital muscular dystrophy patients with dominant and recessive COL6A mutations. Neuromuscul. Disord. *16*, 571–582.

Källberg, M., Wang, H., Wang, S., Peng, J., Wang, Z., Lu, H., and Xu, J. (2012). Template-based protein structure modeling using the RaptorX web server. Nat. Protoc. *7*, 1511–1522.

Kwong, J.Q., and Molkentin, J.D. (2015). Physiological and pathological roles of the mitochondrial permeability transition pore in the heart. Cell Metab. *21*, 206–214.

Lambert, J.P., Luongo, T.S., Tomar, D., Jadiya, P., Gao, E., Zhang, X., Lucchese, A.M., Kolmetzky, D.W., Shah, N.S., and Elrod, J.W. (2019). MCUB Regulates the Molecular Composition of the Mitochondrial Calcium Uniporter Channel to Limit Mitochondrial Calcium Overload During Stress. Circulation *140*, 1720–1733.

Luongo, T.S., Lambert, J.P., Gross, P., Nwokedi, M., Lombardi, A.A., Shanmughapriya, S., Carpenter, A.C., Kolmetzky, D., Gao, E., van Berlo, J.H., et al. (2017). The mitochondrial Na^+/Ca^{2+} exchanger is essential for Ca^{2+} homeostasis and viability. Nature *545*, 93–97.

Mak, S.K., Tewari, D., Tetrud, J.W., Langston, J.W., and Schüle, B. (2011). Mitochondrial dysfunction in skin fibroblasts from a Parkinson's disease patient with an alpha-synuclein triplication. J. Parkinsons Dis. *1*, 175–183.

Morciano, G., Giorgi, C., Bonora, M., Punzetti, S., Pavasini, R., Wieckowski, M.R., Campo, G., and Pinton, P. (2015). Molecular identity of the mitochondrial permeability transition pore and its role in ischemia-reperfusion injury. J. Mol. Cell. Cardiol. *78*, 142–153.

Morciano, G., Sarti, A.C., Marchi, S., Missiroli, S., Falzoni, S., Raffaghello, L., Pistoia, V., Giorgi, C., Di Virgilio, F., and Pinton, P. (2017). Use of luciferase probes to measure ATP in living cells and animals. Nat. Protoc. *12*, 1542–1562.

Morciano, G., Preti, D., Pedriali, G., Aquila, G., Missiroli, S., Fantinati, A., Carroccia, N., Pacifico, S., Bonora, M., Talarico, A., et al. (2018). Discovery of Novel 1,3,8-Triazaspiro[4.5]decane Derivatives That Target the c Subunit of F_1/F_O-Adenosine Triphosphate (ATP) Synthase for the Treatment of Reperfusion Damage in Myocardial Infarction. J. Med. Chem. *61*, 7131–7143.

Morciano, G., Imamura, H., Patergnani, S., Pedriali, G., Giorgi, C., and Pinton, P. (2020). Measurement of ATP concentrations in mitochondria of living cells using luminescence and fluorescence approaches. Methods Cell Biol. *155*, 199–219.

Neginskaya, M.A., Solesio, M.E., Berezhnaya, E.V., Amodeo, G.F., Mnatsakanyan, N., Jonas, E.A., and Pavlov, E.V. (2019). ATP Synthase C-Subunit-Deficient Mitochondria Have a Small Cyclosporine A-Sensitive Channel, but Lack the Permeability Transition Pore. Cell Rep. *26*, 11–17.e2.

Neumann, F.J., Sousa-Uva, M., Ahlsson, A., Alfonso, F., Banning, A.P., Benedetto, U., Byrne, R.A., Collet, J.P., Falk, V., Head, S.J., et al. (2019). 2018 ESC/EACTS Guidelines on myocardial revascularization. EuroIntervention *14*, 1435–1534.

Norris, U., Karp, P.E., and Fimmel, A.L. (1992). Mutational analysis of the glycine-rich region of the c subunit of the Escherichia coli F0F1 ATPase. J. Bacteriol. *174*, 4496–4499.

Ottani, F., Latini, R., Staszewsky, L., La Vecchia, L., Locuratolo, N., Sicuro, M., Masson, S., Barlera, S., Milani, V., Lombardi, M., et al.; CYCLE Investigators (2016). Cyclosporine A in Reperfused Myocardial Infarction: The Multicenter, Controlled, Open-Label CYCLE Trial. J. Am. Coll. Cardiol. *67*, 365–374.

Paradies, V., Chan, M.H.H., and Hausenloy, D.J. (2018). Strategies for Reducing Myocardial Infarct Size Following STEMI. In Primary Angioplasty: A Practical Guide, T.J. Watson, P.J.L. Ong, and J.E. Tcheng, eds. (Springer), pp. 307–322.

Patergnani, S., Giorgi, C., Maniero, S., Missiroli, S., Maniscalco, P., Bononi, I., Martini, F., Cavallesco, G., Tognon, M., and Pinton, P. (2015). The endoplasmic reticulum mitochondrial calcium cross talk is downregulated in malignant pleural mesothelioma cells and plays a critical role in apoptosis inhibition. Oncotarget *6*, 23427–23444.

Pinke, G., Zhou, L., and Sazanov, L.A. (2020). Cryo-EM structure of the entire mammalian F-type ATP synthase. Nat. Struct. Mol. Biol. *27*, 1077–1085.

Piot, C., Croisille, P., Staat, P., Thibault, H., Rioufol, G., Mewton, N., Elbelghiti, R., Cung, T.T., Bonnefoy, E., Angoulvant, D., et al. (2008). Effect of cyclosporine on reperfusion injury in acute myocardial infarction. N. Engl. J. Med. *359*, 473–481.

Portal, L., Martin, V., Assaly, R., d'Anglemont de Tassigny, A., Michineau, S., Berdeaux, A., Ghaleb, B., and Pons, S. (2013). A model of hypoxia-reoxygenation on isolated adult mouse cardiomyocytes: characterization, comparison with ischemia-reperfusion, and application to the cardioprotective effect of regular treadmill exercise. J. Cardiovasc. Pharmacol. Ther. *18*, 367–375.

Santulli, G., Xie, W., Reiken, S.R., and Marks, A.R. (2015). Mitochondrial calcium overload is a key determinant in heart failure. Proc. Natl. Acad. Sci. USA *112*, 11389–11394.

Shanmuganathan, S., Hausenloy, D.J., Duchen, M.R., and Yellon, D.M. (2005). Mitochondrial permeability transition pore as a target for cardioprotection in the human heart. Am. J. Physiol. Heart Circ. Physiol. *289*, H237–H242.

Tesco, G., Vergelli, M., Grassilli, E., Salomoni, P., Bellesia, E., Sikora, E., Radziszewska, E., Barbieri, D., Latorraca, S., Fagiolo, U., et al. (1998). Growth properties and growth factor responsiveness in skin fibroblasts from centenarians. Biochem. Biophys. Res. Commun. *244*, 912–916.

STAR★METHODS

KEY RESOURCES TABLE

REAGENT or RESOURCE	SOURCE	IDENTIFIER
Antibodies		
β-Actin	Merck	Cat# 611222; RRID:AB_398754
TIM23	BD	Cat# 611222; RRID:AB_398754
MCU	Merck	Cat# HPA016480; RRID: AB_2071893
MCUb	Merck	Cat# HPA048776; RRID: AB_2680518
MICU1	Merck	Cat# HPA037480; RRID: AB_10696934
ATP5I	Abcam	Cat# ab122241; RRID: AB_11127890
ATP5L	Abcam	Cat# ab126181; RRID: AB_11129974
Csub	Abcam	Cat# ab181243; RRID: AB_181243
CypD	Abcam	Cat# ab110324; RRID: AB_10864110
Total OXPHOS	Abcam	Cat# ab110413; RRID: AB_2629281
ACO1	Abcam	Cat# ab183721; RRID: AB_183721
ACO2	Cell signaling	Cat# 6922; RRID: AB_10828218
SDHA	Abcam	Cat# 137756; RRID: AB_137756
ATP5A	Abcam	Cat# ab14748; RRID: AB_301447
ATP5B	Santa Cruz	Cat# sc-166443; RRID: AB_2061895
ATP5O	Abcam	Cat# ab110276; RRID: AB_10887942
Chemicals, peptides, and recombinant proteins		
2-Propanol	Merck	33539
Ethanol	Merck	51976
G418 disulfate salt	Merck	A1720
Calcein, AM	Thermo Fisher Scientific	C3100MP
Cobalt(II) chloride hexahydrate	Merck	C8661
Ionomycin calcium salt	Merck	I0634
Tetramethylrhodamine, Methyl Ester, Perchlorate (TMRM)	Thermo Fisher Scientific	T668
Carbonyl cyanide 4-(trifluoro-methoxy)phenylhydrazone	Merck	C2920
MitoTracker Deep Red FM	Thermo Fisher Scientific	M22426
Triton X-100 for molecular biology	Merck	T8787
Bovine Serum Albumin	Merck	A4503
Calcium Chloride solution	Merck	21115
HEPES	Merck	H3375
Potassium Chloride	Merck	P5405
Sodium Chloride	Merck	S7653
Magnesium chloride hexahydrate	Merck	M2670
Sodium phosphate	Merck	342483
Magnesium sulfate heptahydrate	Merck	M5921
D-(+)-Glucose	Merck	G7021
Bradykinin acetate salt	Merck	B3259
Histamine dihydrochloride	Merck	H7250
Fura-2, AM	Thermo Fisher Scientific	F1221
Pluronic® F-68	Merck	P1300
(±)-Sulfinpyrazone 5G	Merck	S9509
Ethylenediaminetetraacetic acid	Merck	E6758
Acetic acid	Merck	695092
Crystal Violet	Merck	C0775

(*Continued on next page*)

Continued

REAGENT or RESOURCE	SOURCE	IDENTIFIER
Oligomycin from Streptomyces diastatochromogenes	Merck	O4876
Rotenone	Merck	R8875
Antimycin A from Streptomyces sp.	Merck	A8674
Digitonin	Merck	300410
Annexin V-FITC conjugated	Thermo Fisher Scientific	A13199
Propidium Iodide	Thermo Fisher Scientific	P3566
Critical commercial assays		
The Proteasome Activity Assay Kit	Abcam	ab107921
Seahorse XF Cell Mito Stress Test Kit	Agilent	103015-100
Experimental models: cell lines		
AC16	Merck	Cat# SCC109; RRID: CVCL_4U18
Fibroblasts	Patients	N/A
Oligonucleotides		
F-tacaccttggtcgccatctt R-gagcagtgggtcttcaaagc	This study	ATP5G1-5′UTR
F-cctttcgcaacatttccttc R-gctgtctctatggccaggac	This study	ATP5G1-1
F-tgattaaagctgtgcccaaa R-ggagtgcagtggcatagtca	This study	ATP5G1-2
F-ccaaagtgggaggagagttg R-aggacacaggagggtgaggt	This study	ATP5G1-3
F-ggaggagctcccttcagga R-actcagacaaacccatattcctc	This study	ATP5G1-4
F- atccagtgatgccagagtcc R- gactgggtggaacaggtgaa	This study	ATP5G2-1
F- aagtcttgagaagcgttccttt R- ctgttgcctcagcctcct	This study	ATP5G2-2
F- tgttgagtgaggcaaatgct R- tgaggccctagtctattcttgc	This study	ATP5G2-3
F- cctgtgcactgctgctaact R- atcgcttgaacccagaggta	This study	ATP5G2-4
F- gggccaagaggtcttaatttg R- ttcgggccttgtactctcac	This study	ATP5G2-5
F- ccggctagttgccaataaag R- aaagggccactcctggtcta	This study	ATP5G3-1
F- ttcaaggtagcaagcgttacaa R- gtcaagcaatcctccctcct	This study	ATP5G3-2
F- tgacagaccaggtgagacctt R- gacctgggcaagtaatgtgg	This study	ATP5G3-3
F- cagatggataagaatgtcagaacc R- gcttcctctgaatgggacag	This study	ATP5G3-4
Recombinant DNA		
ATP5G1^{WT} plasmid	This study	N/A
ATP5G1^{G87E} plasmid	This study	N/A
mtLUC	PMID: 28683062	N/A
2 mt-GCAMP	PMID: 26538029	N/A
Software and algorithms		
ImageJ	National Institute of Health (NIH)	RRID: SCR_003070; https://imagej.net/Welcome
GraphPad	GraphPad	RRID: SCR_000306; https://www.graphpad.com
PolyPhen-2	PolyPhen-2	RRID: SCR_013189; http://genetics.bwh.harvard.edu/pph2/
RaptorX	UChicago	RRID: SCR_018118; http://raptorx.uchicago.edu

RESOURCE AVAILABILITY

Lead contact

Further information and requests for resources and reagents should be directed to and will be fulfilled by the lead contact, Paolo Pinton (paolo.pinton@unife.it).

Materials availability

Reagents generated in this study will be made available on request, but we may require a completed materials transfer agreement.

Data and code availability

Data are available upon request.

EXPERIMENTAL MODEL AND SUBJECT DETAILS

AC16 and fibroblasts cells

The AC16 human cardiomyocyte cell line was grown in DMEM/F12 containing 2 mM L-glutamine, 12.5% FBS and 1x PS solution. AC16 stable clones overexpressing wild-type or mutated c subunit were grown in the same DMEM/F12 supplemented with 0.4 mg/ml G418 selection. Human primary fibroblasts were grown in DMEM supplemented with 20% FBS, 2 mM L-glutamine and 1x PS.

STEMI patients

To investigate the potential role of genetic determinants a complete analysis of the gene coding for the c subunit was performed in 52 out of 158 previously enrolled by us (Campo et al., 2016). It was a single-center, investigator-driven, prospective study conducted at the Cardiology Unit of the Azienda Ospedaliero Universitaria di Ferrara, Ferrara, Italy. Patients were enrolled between December 2013 and January 2015. The inclusion and exclusion criteria have been previously reported (Campo et al., 2016). Age: 63 ± 11; Gender: 39 males and 13 females.

For the second study, it was a single-center, investigator-driven, prospective study conducted at the Cardiology Unit of the Azienda Ospedaliero-Universitaria di Ferrara (Ferrara, Italy). Patients were enrolled between February 2019 and March 2019. The trial was performed according to the Declaration of Helsinki and approved by the local ethics committee (Comitato Etico Unico della Provincia di Ferrara). The inclusion criteria for enrollment were as follows: i) first-time acute anterior ST-segment elevation myocardial infarction (STEMI) treated with successful PCI; ii) time from onset of symptoms to balloon < 6 h; iii) culprit lesion in the proximal or mid portion of the left anterior descending artery (LAD); and iv) baseline thrombolysis in myocardial infarction (TIMI) flow 0–1. Age: 58 ± 7; Gender: 13 males and 1 female.

No confounding factors (sex, gender, comorbidities) were found to influence the results.

METHOD DETAILS

C subunit genetic screening

To investigate the potential role of genetic determinants in intersubject variability, a complete analysis of the gene coding for the c subunit of the mitochondrial permeability transition pore was performed in 52 out of 158 previously enrolled by us (Campo et al., 2016). It was a single-center, investigator-driven, prospective study conducted at the Cardiology Unit of the Azienda Ospedaliero Universitaria di Ferrara, Ferrara, Italy. Patients were enrolled between December 2013 and January 2015. The inclusion and exclusion criteria have been previously reported (Campo et al., 2016) and identical to those of study B. The aim of the study was to measure the values of the serum C subunit and to correlate them with surrogate markers of reperfusion injury. In 52 of these patients, whole blood was available for DNA extraction and was considered for the present analysis. DNA was extracted, and full sequencing of the C subunit gene was performed.

Blood sample collection

Blood withdrawal was performed 6–18 h after the end of successful PCI (median 10 [8–13] h). Blood samples were collected from an antecubital vein using a 21-gauge needle. The first 2 to 4 mL of blood was discarded. The remaining blood was collected in empty tubes and, after 45 min, centrifuged at 1700 g at 4°C for 15 min. The serum obtained was stored at −20°C.

DNA extraction

Genomic DNA was extracted from the whole blood of selected patients after providing informed consent. The Wizard® Genomic DNA Purification Kit (Promega) was used according to the manufacturer's instructions (https://www.promega.com/-/media/files/resources/protcards/wizard-genomic-dna-purification-kit-quick-protocol.pdf?la=en).

Briefly, 900 μl of cell lysis solution was added to 300 μl of whole blood; samples were incubated for ten minutes at room temperature and centrifuged at 19000 g for 20 s. The supernatant was discarded, the pellet was vortexed before, 300 μl of nuclei lysis solution was added and mixed by inversion, and finally, 100 μl of protein precipitation solution was added. The obtained solution was vortexed for 20 s and centrifuged at 19000 g for three minutes.

The supernatant was transferred to a new tube containing 300 μl of isopropanol, mixed and centrifuged at 19000 g for one minute. The supernatant was discarded, and the DNA pellet was washed with 70% ethanol and centrifuged, as described above. After removal of the ethanol, the DNA pellet was air-dried and resuspended in 100 μl of DNase-free water.

PCR amplification, sequencing and analysis

Primers were designed to amplify approximately 200 base pairs before and after all exons and UTRs of the ATP5G1, ATP5G2 and ATP5G3 genes using Primer3Plus online software (http://www.bioinformatics.nl/cgi-bin/primer3plus/primer3plus.cgi).

PCR amplification was performed using the AmpliTaq Gold® 360 kit (Life Technologies) and 50 ng of genomic DNA per reaction. The full list of PCR primers and annealing temperatures are available in Table S2. After verification on agarose gel, amplicons were purified in Microcon Millipore columns and sent for sequencing to Macrogen Europe (https://dna.macrogen.com). Chromatograms were visualized with Chromas (version 2.33) and analyzed with Blast and Lasergene SeqMan (version 7.0.0 Build) allowing multiple alignments and direct comparison of several sequences at the same time. The identified variants were compared with dbSNP139 (https://www.ncbi.nlm.nih.gov/snp/) and are reported in Table 1.

Predictive software

PolyPhen-2 (Polymorphism Phenotyping v2) was used to predict the possible impact of an amino acid substitution on the structure and function of the Csub protein using straightforward physical and comparative considerations, as described in Adzhubei et al. (2013). Similarly, RaptorX was used to predict secondary and tertiary protein structures, contact and distance maps, as described in Källberg et al. (2012).

Cell culture and transient transfection

The AC16 human cardiomyocyte cell line (Merck-Millipore, cod. SCC109) was grown in DMEM/F12 containing 2 mM L-glutamine, 12.5% FBS and 1x PS solution in 75-cm^2 Corning flasks. AC16 stable clones overexpressing wild-type or mutated c subunit were grown in the same DMEM/F12 supplemented with 0.4 mg/ml G418 selection. Human primary fibroblasts were grown in DMEM supplemented with 20% FBS, 2 mM L-glutamine and 1x PS in 100 mm Petri dishes. All cells were maintained at 37°C under 90% relative humidity in 5% CO_2. Before transfection or infection, cells were seeded onto 13-mm glass coverslips for intracellular Ca^{2+} measurements and onto 24-mm glass coverslips for microscopic analysis. All experiments were performed 24 h after plasmid transfections with Lipofectamine 2000. In experiments involving compound 10, cells were pretreated for 15 min with a 5 μM concentration of the compound in complete medium. Cells were used at p3-p9 for AC16 and p3-p6 for fibroblasts.

Hypoxia/reoxygenation protocol

Where needed, cells were rinsed with PBS, and the culture medium was changed according to the oxygen-glucose deprivation protocol described in Portal et al. (2013) with slight variation. Cells were exposed to 1% O_2 at 37°C for 12 h to simulate ischemia. At the time of reperfusion, cells were cultured with complete fresh medium and measured 6 h later.

PTPC measurements

For the calcein-cobalt quenching assay, all cells were loaded with 1 μM calcein acetoxymethyl ester and 2 mM Co^{2+}, and staining solution was added to cells for 15 min at 37°C in a 5% CO_2 atmosphere (Bonora et al., 2016; Portal et al., 2013). Image acquisition was performed with a Nikon Eclipse Ti confocal microscope with a 40 × /0.60 SPlanFluor objective. The rate of PTPC opening was determined as the slope of the calcein fluorescence trace over a period of 60 s poststimulation with 500 nM ionomycin administered 30 s after the beginning of the experiment to induce PTPC opening. For mitochondrial membrane potential measurements, cells were loaded with 20 nM tetramethylrhodamine methyl ester (TMRM) for 30 min at 37°C. Stimulation with 500 μM H_2O_2, a pro-oxidant, induced PTPC opening and mitochondrial depolarization and reduced TMRM signal intensity (Bonora et al., 2016). Image acquisition was performed with a Nikon Eclipse Ti confocal microscope with a 40 × /0.60 SPlanFluor objective.

Basal mitochondrial membrane potential

Cells were loaded with 20 nM tetramethylrhodamine methyl ester (TMRM) for 30 min at 37°C. To obtain and analyze basal levels, cells were stimulated with 10 nM carbonyl cyanide p-trifluoromethoxyphenylhydrazone (FCCP), a strong uncoupler of oxidative phosphorylation.

Mitochondrial morphology

Primary fibroblasts were stained with 20 nM MitoTracker Deep Red FM for 30 min at 37°C and imaged with a Nikon Eclipse Ti confocal microscope using a 60 × 1.4 NA Plan-Apochromat oil-immersion objective. The analysis was performed with IMARIS software.

Immunofluorescence

AC16 cells were grown on 13-mm coverslips and transfected as described previously, washed with PBS and fixed in 4% formaldehyde for 10 min at 37°C. After washing three times with PBS, cells were permeabilized with 0.1% Triton X-100 in PBS (PBS-T) for 2 h at room temperature and then blocked with PBS-T containing 2% BSA at room temperature for 1 h. For fibroblasts, permeabilization lasted 10 min with 0.05% PBS-T. Cells were then incubated with primary antibodies overnight at 4°C, washed 3 times with PBS-T, and incubated with the appropriate isotype-matched AlexaFluor-conjugated secondary antibodies. Coverslips were mounted with mounting medium and DAPI reagent at room temperature, and images were acquired with a Nikon Eclipse Ti confocal microscope using a 60 × 1.4 NA Plan-Apochromat oil-immersion objective. Acquired images were then analyzed by using open-source Fiji software.

Annexin-V and Propidium iodide assays

After H/R, AC16 cells were stained according to the manufacturer's protocols with Annexin V-FITC conjugated (Thermo Fisher Scientific, A13199) and PI (Thermo Fisher Scientific, P3566) in binding buffer (10 mM HEPES, 5 mM KCl, 150 mm NaCl, 1.8 mM $CaCl_2$, 1 mM $MgCl_2$, pH 7.4) and left in the dark at room temperature for 15 min. Annexin V-FITC- and PI-positive cells were quantified by flow cytometry (Attune Nxt Flow cytometer, Thermo Fisher Scientific), and data were analyzed with Attune Nxt Software (Thermo Fisher Scientific).

Ca^{2+} measurements

Fibroblasts were infected with mtAEQmut, and AC16 cells were transfected with either mtAEQwt or cAEQ. Forty-eight hours later, the coverslips were incubated with 5 μM coelenterazine for 1.5 h in Krebs-Ringer modified buffer (KRB) supplemented with 1 mM $CaCl_2$ (KRB: 125 mM NaCl, 5 mM KCl, 1 mM Na_3PO_4, 1 mM $MgSO_4$, 5.5 mM glucose, and 20 mM HEPES, pH 7.4, at 37°C). Aequorin signals were measured in KRB supplemented with 1 mM $CaCl_2$ using a purpose-built luminometer. The agonist (500 μM bradykinin for fibroblasts and a mix of 500 μM bradykinin and histamine for AC16) was added to the same medium. The experiments were terminated by lysing the cells with Triton X-100 in a hypotonic Ca^{2+}-rich solution (10 mM $CaCl_2$ in H_2O), thus discharging the remaining aequorin pool. The light signals were collected and calibrated with [Ca^{2+}] values. Further experimental details have been previously described in Bonora et al. (2013b).

FURA-2 AM: basal cytosolic Ca^{2+} and its response upon agonist administration was evaluated essentially as described in Patergnani et al. (2015), making use of the fluorescent Ca^{2+} indicator Fura-2 AM (Life Technologies, Invitrogen). Briefly, cells were grown on 24-mm coverslips and incubated at 37°C for 30 min in 1 mM Ca^{2+}/Krebs-Ringer buffer supplemented with 2.5 μM Fura-2/AM, 0.02% Pluronic F-68 (Sigma), and 0.1 mM sulfinpyrazone (Sigma). To determine the basal cytosolic Ca^{2+} ratio, cells were placed in an open Leyden chamber on a 37°C thermostated stage and exposed to 340/380 nm wavelength light in resting conditions; to evaluate its response to agonists, histamine (His) and bradykinin (BK) were added to 1 mM Ca^{2+}/Krebs-Ringer buffer, and the Ca^{2+} ratio increase in the cytosol was recorded as indicated in the figures. The fluorescence data collected were expressed as emission ratios at 340/380 nm.

2 mt-GCAMP: To test resting mitochondrial Ca^{2+} concentrations with high sensitivity, we used a new Ca^{2+} probe based on the last-generation GCaMP targeted to the mitochondrial matrix. We chose the GCaMP6 m version because it had the highest Ca^{2+} affinity. To measure the signal independent of variations in basal fluorescence intensity due to the variable expression levels of the probe, we took advantage of the isosbestic point in the GCaMP6 m excitation spectrum; exciting GCaMP6 m at 406 nm led to fluorescence emission that was not Ca^{2+} dependent. As a consequence, the ratio between the excitation wavelengths of 494 and 406 nm was proportional to the Ca^{2+} concentration and independent of probe expression levels. Cells were imaged with an IX-81 automated epifluorescence microscope (Olympus) equipped with a 40 × oil immersion objective (numerical aperture 1.35; Olympus) and an ORCA-R2 charge-coupled device camera (Hamamatsu Photonics).

Proximity ligation assay (PLA)

After fixation, cells were exposed to 1 mM EDTA buffer (pH 8.0) for 20 min at 100°C (antigen retrieval), and the procedure was started. The PLA protocol to detect F_1F_O ATP synthase dimers is described in detail in (Bonora et al., 2017). Protein proximity was evaluated on a Nikon Eclipse Ti confocal microscope using a 60 × 1.4 NA Plan-Apochromat oil-immersion objective.

Immunoblot analysis

For immunoblotting, cells were lysed in RIPA buffer and then quantified by the Lowry method, and 10 μg of protein was loaded on a 4%–20% precast gel. After electrophoretic separation, proteins were transferred onto nitrocellulose membranes that were incubated overnight with the following primary antibodies: β-Actin (Merck, A1978, 1:5000), TIM23 (BD Biosciences, 611222, 1:1000), MCU (Merck, HPA016480, 1:1000), MCUb (Merck, HPA048776, 1:1000), MICU1 (Abcam, HPA037480, 1:1000), ATP5I (Abcam, ab122241, 1:1000), ATP5L (Abcam, ab126181, 1:1000), CypD (Abcam, ab110324, 1:1000), Csub (Abcam, ab181243, 1:1000), Total OXPHOS WB Antibody Cocktail (Abcam, ab110413, 1:250), ACO1 (Abcam, ab183721, 1:1000), ACO2 (Cell signaling, 6922, 1:1000), SDHA (Abcam, ab137756, 1:1000) The membranes were then treated with specific HRP-labeled secondary antibodies, followed by chemiluminescence detection using a ChemiDoc Touch Gel Imaging System.

Cell viability assay (Crystal violet)

Cells seeded in 12-well plates were treated with the I/R protocol in the presence or absence of compound 10. Then, the cells were washed with PBS, fixed in 4% paraformaldehyde, and stained with 0.1% crystal violet. Crystal violet was dissolved in 1 mol/L acetic acid, and the absorbance at 590 nm was measured with a spectrophotometer.

Oxygen Consumption Rate

The rate of oxygen consumption was assayed with an XF96 Extracellular Flux Analyzer (Seahorse Biosciences—Agilent Technologies, Santa Clara, CA USA). Briefly, mitochondrial respiration was evaluated by measuring the OCR under basal conditions and after the addition of oligomycin (1 μM), carbonyl cyanide-4-(trifluoromethoxy)phenylhydrazone (FCCP) (2 μM), rotenone (1 μM) and antimycin A (1 μM). OCR values were normalized to cell density using the crystal violet assay.

Luciferine-luciferase assay

Experiments were carried out as previously described in Morciano et al. (2017).

Briefly, AC16 cells expressing a mitochondrially targeted variant of Photinus pyralis luciferase were perfused with Krebs-Ringer modified buffer (KRB) supplemented with 1 mM $CaCl_2$ (KRB: 125 mM NaCl, 5 mM KCl, 1 mM Na_3PO_4, 1 mM $MgSO_4$, 5.5 mM glucose, and 20 mM HEPEs, pH 7.4, at 37°C), and luciferin-dependent luminescence was monitored with a customized luminometer (Elettrofor). The experiments started with background acquisition in which cells were perfused with only KRB solution. Then, KRB supplemented with 25 μM luciferin was added to reach the plateau.

Cellular Thermal Shift Assay (CETSA)

CETSA was performed as described in a previous publication (Morciano et al., 2018). Briefly, cells from both experimental conditions were detached and pelleted by centrifugation at 1,300 rpm for 5 min. The cells were resuspended in EBC buffer and divided into equal amounts. Subsequently, the samples were exposed to increasing temperatures ranging from 53°C to 80°C, stabilized at RT and lysed by 2 cycles of incubation in liquid nitrogen. Next, the samples were pelleted at 13,200 rpm for 15 minutes. Supernatants were analyzed by immunoblots using antibodies against Flag-tagged and MCU proteins after SDS-PAGE. CETSA curves were obtained by quantifying immunoblot bands and converting the data into percentages.

Proteasome activity assay kit

The Proteasome Activity Assay Kit (Fluorometric, ab107921) takes advantage of chymotrypsin-like activity, utilizing an AMC-tagged peptide substrate that releases free, highly fluorescent AMC in the presence of proteolytic activity. Briefly, cells were harvested and resuspended in 0,5% NP-40 lysis buffer and centrifuged at 13,000 rpm for 10 min. Supernatants and positive controls (with and without proteasome inhibitor) were placed in a dark glass 96-multiwell plate and completed with proteasome substrate. Fluorescence at 350/444 nm was acquired for 60 min by a GloMax plate reader (Promega).

Blue-native PAGE and in gel activity assay

Briefly, cells were harvested, resuspended in PBS (with Ca^{2+} and Mg^{2+}) and centrifuged at 200 x g for 3 minutes at room temperature. Cell pellets were resuspended in 1 mL of ice-cold homogenization medium (75 mM sucrose, 225 mM mannitol, 0.1 mM EGTA, 50 mM Tris-HCl pH 7.4.) and homogenized in a motor-driven tightly fitting glass/Teflon Potter Elvehjem homogenizer. Homogenates were centrifuged at 16000x g for 15 minutes at 4°C. Supernatants were discarded, and the membrane-enriched pellets were resuspended in of BN sample buffer (50 mM Bis-Tris, 1 M 6-aminohexanoic acid (pH 7.0)). Protein content in the samples was measured with the use of Protein Assay Dye Reagent Concentrate (Bio-Rad) according to the manufacturer protocol. Next, digitonin 3 mg:1 mg protein (digitonin:protein ratio) was added to the samples. After the native lysates were incubated on ice for 30 minutes, they were centrifuged at 8000 g for 10 minutes to remove insolubilized material. Protein content in the native lysates was measured with the use of Protein Assay Dye Reagent Concentrate (Bio-Rad). Thereafter, native lysates were combined with Serva Blue G (5% suspension in 500 mM 6-aminohexanoic acid) to set the ratio of 8 mg detergent:1 mg Coomassie. Next, 60 or 100 μg of protein was loaded and separated on a freshly prepared 6% polyacrylamide native gel. As an internal standard, 40 μg of sample prepared from rat heart mitochondria was used. The gel ran with a constant voltage at 75 V for 30 minutes. After 30 minutes, the cathode buffer containing Serva Blue G was replaced by the fresh cathode buffer Serva Blue G – free, and the voltage was increased up to 150 V until the blue front line reached the bottom of the gel.

To visualize monomeric and dimeric forms of ATP synthase, native gels were preincubated for 1 hour in a buffer containing 35 mM Tris and 270 mM glycine, pH 7.8. Following removal of the incubation solution, the gels were next incubated in ATP-ase assay buffer containing 35 mM Tris, 300 mM glycine, 14 mM $MgSO_4$, 0.2% Pb_2NO_3, and 9 mM ATP, pH 7.8. ATP hydrolysis correlated with the development of white lead phosphate precipitates. The reaction was stopped using 50% methanol for 30 min, and then the gels were transferred to water and scanned for densitometric quantification.

The level of ATP synthase in the native lysates (used for the gel activity assay) was evaluated with the WB technique. Native lysate samples used for BN electrophoresis (50 μg/lane) were mixed with reducing Laemmli loading buffer and denatured at 37°C for 5 min according to the requirements of the antibodies. Protein samples were separated on 10% polyacrylamide gels and transferred to nitrocellulose membranes. Equal protein loading was evaluated with reversible Ponceau staining. The membranes were incubated for 5 minutes in 0.1% Ponceau solution in (w/v) 5% acetic acid; afterward, the membranes were washed with deionized water and scanned. Ponceau staining was removed by incubation of the membranes in TBS supplemented with 0.1% Tween (TBS-T). Thereafter, membranes were blocked using 5% nonfat milk (Blotting-Grade Blocker, Bio-Rad) in TBS-T, followed by incubation with MitoProfile®Total OXPHOS Human WB (ab110411) primary antibodies cocktail overnight (1:2,000 in 2.5% nonfat milk in TBS-T). Next, the membranes were washed with TBS-T and incubated with secondary donkey anti-mouse antibodies labeled with IR-Dye®800CW (Li-Cor, Biosciences) (1:5,000 in 2.5% nonfat milk in TBS-T). The relative levels of the ATP5A subunit (corresponding complex V level) and UQCRC2 subunit (corresponding complex III level) on the membranes were visualized using an Odyssey infrared imaging system (Li-Cor Biosciences with fluorescent objectives). The fluorescence intensity of the membranes was analyzed using Image Studio Lite software version for Odyssey® 3021, which is compatible with the Odyssey infrared imaging system.

Analysis of F_1-ATP synthase proteins

Mitochondria from AC16 cells (both control and 1 h 1 μM ionomycin-treated conditions) were isolated by conventional procedures involving differential centrifugation as described in our previous publications. F_1 mitochondrial proteins were analyzed with WB by detecting ATP5A (Abcam, 14748, 1:5000), ATP5B (Santa Cruz, 166443, 1:500), and ATP5O (Abcam, 110276, 1:1000).

Study population for PTPC function and reperfusion damage tests and C subunit genetic screening

The study was a single-center, investigator-driven, prospective study conducted at the Cardiology Unit of the Azienda Ospedaliero-Universitaria di Ferrara (Ferrara, Italy). Patients were enrolled between February 2019 and March 2019. The trial was performed according to the Declaration of Helsinki and approved by the local ethics committee (Comitato Etico Unico della Provincia di Ferrara). The inclusion criteria for enrollment were as follows: i) first-time acute anterior ST-segment elevation myocardial infarction (STEMI) treated with successful PCI; ii) time from onset of symptoms to balloon < 6 h; iii) culprit lesion in the proximal or mid portion of the left anterior descending artery (LAD); and iv) baseline thrombolysis in myocardial infarction (TIMI) flow 0–1.

The major exclusion criteria were prior myocardial infarction and/or percutaneous or surgical coronary revascularization and/or prior angina and/or evidence of ischemic heart disease, previous heart failure, cardiac arrest and/or cardiogenic shock, atrial fibrillation, pacemaker, concurrent inflammatory, infectious or malignant disease, liver and/or renal failure, recent significant bleeding and/or major surgery (< 4 weeks), or the use of oral anticoagulants or contraceptives. The PCI procedure, antithrombotic drugs and all other medications were administered according to standard guideline-driven clinical practice, following institutional protocols (Neumann et al., 2019). The study flow comprised a skin biopsy to obtain fibroblasts and a cMRI to assess the reperfusion injury.

Skin biopsy

Skin biopsies (3 mm punch) were collected from the volar side of the forearm (Tesco et al., 1998). Each biopsy was cut into small pieces (approximately 0.5 mm) and seeded in 25 cm^2 flasks (Tesco et al., 1998). The tissue was collected with a clamp and transferred to a sterile container prefilled with an adequate quantity of preservative solution.

Cardiac MRI

All cMRI studies were performed with a 1.5-T scanner (Signa HDX, GE Medical Systems, Milwaukee, Wisconsin) using dedicated cardiac software, a phased-array surface receiver coil and ECG triggering. Patients underwent cMRI at two different time points: the first cMRI was performed within 4 ± 1 days, and the second cMRI was performed 180 ± 20 days after successful primary PCI. Data were analyzed using Segment software (Medviso, Svezia) by an operator fully blinded to the study protocol. After acquisition of localizer images, cine images were obtained using breath-hold single-phase steady-state free precession (SSFP) sequences in multiple short-axis and 3 long-axis views (slice thickness 10 mm, no gap in identical slice positions). A black-blood T2-weighted short inversion time inversion-recovery fast spin echo sequence was utilized in the same views as the cine sequences to evaluate myocardial edema. Ten minutes after intravenous injection of contrast agent (0.15 mmol/kg gadobutrol, Scering, Germany), late gadolinium enhancement (LGE) images were acquired using a breath-hold segmented T1-weghted inversion-recovery gradient-echo sequence in the same long-axis and short-axis views as the cine images. The inversion time was individually adjusted to null normal myocardium. T2-weighted and LGE images were semiautomatically analyzed. Infarct-related edema was defined by a signal intensity > 2 standard deviations (SDs) of the mean signal intensity of the noninfarcted myocardium, identifying the area at risk (AAR) expressed as a percentage of the LV mass. Infarcted myocardium was quantified on LGE images as myocardium with a signal intensity exceeding the mean signal intensity of remote myocardium by at least 5 SD and was expressed as a percentage of the LV mass. Finally, the myocardial salvage index (MSI) was calculated according to the equation (AAR-infarct size at LGE)/AAR) and was expressed as a value ranging between 0 and 1 (Eitel et al., 2010).

QUANTIFICATION AND STATISTICAL ANALYSIS

The statistical methods included t tests (when comparing two experimental groups), one-way ANOVA with or without multiple comparisons (for three or more groups) and Spearman's correlation coefficient r calculated by GraphPad Prism. Results with a p value lower than 0.05 were considered significant; ***$p < 0.001$, **$p < 0.01$, *$p < 0.05$ compared to controls. Each experiment was repeated at least three times. For details and information about specific experiments, please refer to Figure Legends.